CO_2 REFORMING OF METHANE OVER Zr-PROMOTED Ni/SBA-15 CATALYST: EFFECT OF ZIRCONIUM LOADING

HARRYDASS A/L ELLAPAN
DR.NURUL AINI BINTI MOHAMED RAZALI

BACHELOR OF CHEMICAL ENGINEERING
UNIVERSITI MALAYSIA PAHANG

CO_2 REFORMING OF METHANE OVER Zr-PROMOTED Ni/SBA-15 CATALYST: EFFECT OF ZIRCONIUM LOADING

HARRYDASS A/L ELLAPAN

Thesis submitted in partial fulfilment of the requirements
For the award of the degree of
Bachelor of Chemical Engineering

Faculty of Chemical & Natural Resources Engineering
UNIVERSITI MALAYSIA PAHANG

DECEMBER 2016

UNIVERSITI MALAYSIA PAHANG

DECLARATION OF THESIS AND COPY RIGHT

Author's Full Name : _____

Date of Birth : _____

Title _____

_____

_____

Academic Session : _____

I declared that this thesis is classified as:

☐ **CONFIDENTIAL** (Contains confidential information under the Official Secret Act 1972)*

☐ **RESTRICTED** (Contains restriction information as specified by the organization where research was done)*

■ **OPEN ACCESS** I agree that my thesis to be published as online open access (Full text)

I acknowledge that University Malaysia Pahang reserve the right as follows:

1. The Thesis is the Property of University Malaysia Pahang.
2. The Library of University Malaysia Pahang has right to make copies for the purpose of research only.
3. The Library has the right to make copies of the thesis for academic exchange.

Certified By:

_____	_____
(Student's Signature)	(Supervisor's Signature)
_____	_____
New IC /Passport Number:	Name of Supervisor:
Date:	Date:

NOTES : *If the thesis is CONFIDENTIAL or RESTRICTICTED, please attach with the letter from the organization with period and reasons for confidentiality or restriction.

SUPERVISOR'S DECLARATION

We hereby declare that we have checked this thesis and in our opinion, this thesis is adequate in terms of scope and quality for the award of the degree of Bachelor of Chemical Engineering.

Signature	:
Name of main supervisor	: DR.NURUL AINI BINTI MOHAMED RAZALI
Position	: SENIOR LECTURER
Date	: 15th DECEMBER 2016

STUDENT'S DECLARATION

I hereby declare that the work in this thesis is my own except for quotations and summaries which have been duly acknowledged. The thesis has not been accepted for any degree and is not concurrently submitted for award of other degree.

Signature :
Name : HARRYDASS A/L ELLAPAN
ID Number : KA 13110
Date : 15th DECEMBER 2016

Dedication

To my parents, lecturers, and God.

ACKNOWLEDGEMENT

I would like to express my special appreciation and thanks to my supervisor, Dr. Nurul Aini Binti Mohamed Razali for her patience, guidance and mentorship. Her knowledge and undying support and encouragement were the main drive for me to complete this thesis successfully. My fullest appreciation goes as well to my senior colleagues, Miss. Nasuha and Miss Syahida for their ideas and support from the beginning till the end of my research.

A special thanks to my family. Words cannot express how grateful I am to my mother, father, mother-in law and father-in-law for the love and support throughout these years. Your prayer for me was what sustained me thus far. I would like express appreciation to my beloved husband who always be my support in the moments when there was no one to answer my queries and for all the sacrifices you have made on my behalf.

I am also indebted to the Ministry of Higher Education and Universiti Malaysia Pahang for funding my study. I would also like to thank all of my friends who supported me in writing, and motivate me to strive towards my goal. I am sincerely grateful to the staffs of Chemical Engineering and Natural Resources Faculty who helped me in many ways and made my stay in UMP pleasant and unforgettable.

ABSTRACT

In the present time, increased concerns on anthropogenic greenhouse gas emissions and abundance of natural gas resources have renewed interest in the CO_2 (dry) reforming process as an alternative to steam reforming for synthesis gas production from natural gas. The catalytic performance of catalyst is considered the most crucial field of study in CO_2 reforming of methane. Various researches were conducted in order to optimize the conversion and minimize the deactivation rate of catalyst. In this research, the effect of Zirconium promoter on the Ni/SBA-15 catalyst at normal reaction temperature of CO_2 reforming of methane had been carried out using a continuous-flow fixed-bed quartz reactor. A series of Zirconium promoted Ni/SBA-15 catalyst with different Zirconium contents (1, 3, 5, 7 wt %) prepared using modified sol-gel method. In addition, the catalyst samples with different Zirconium loadings characterized using BET surface measurement, Fourier Transform Infrared Spectroscopy (FTIR), X-Ray Diffraction (XRD) and Thermal Gravimetric Analysis (TGA). The synthesized Zr/Ni/SBA-15 catalyst tested for CO_2 reforming of methane. This reaction is considered to be a great alternative to produce synthesis gas since it utilizes two abundant greenhouse gases. CO_2 reforming of methane yields low hydrogen to carbon monoxide (H_2/CO) ratio, which is desirable for many industrial synthesis processes. On the other hand, Zirconium promoted Nickel species enhances the formation of active center for the reaction. As a result, the promoted catalyst with 1wt% of Zr perform with optimum catalytic activity and producing higher amount of H_2 at reaction temperature of 800^oC compared to others. Zirconium species is well dispersed and promote the Nickel to be confined to the pores of SBA-15. The wall of SBA-15 limited the sintering of the Ni components. Thus, the Nickel species not undergone sintering as it is well embedded to SBA-15 which can withstand higher temperature.

Keywords: Dry reforming, synthesis gas, Zirconium series promoter, sol-gel method, SBA-15

ABSTRAK

Pada masa ini, peningkatan kebimbangan mengenai pelepasan gas rumah hijau antropogenik dan kaya dengan sumber gas asli telah memperbaharui minat CO2 (kering) proses pembaharuan sebagai alternatif kepada pembentukan semula stim untuk pengeluaran gas sintesis daripada gas asli. Prestasi pemangkin pemangkin dianggap bidang yang paling penting dalam kajian CO2 pembaharuan metana. Pelbagai kajian telah dijalankan untuk mengoptimumkan penukaran dan mengurangkan kadar penyahaktifan daripada pemangkin. Dalam kajian ini, kesan zirkonium promoter pada pemangkin Ni / SBA-15 pada suhu tindak balas normal CO2 pembaharuan metana telah dijalankan menggunakan berterusan aliran katil tetap reaktor kuarza. Satu siri zirkonium dinaikkan pangkat Ni / SBA-15 pemangkin dengan kandungan zirkonium yang berbeza (1, 3, 5, 7% berat) disediakan dengan menggunakan diubahsuai kaedah sol-gel. Di samping itu, sampel pemangkin dengan beban zirkonium yang berbeza mempunyai ciri-ciri menggunakan pengukuran permukaan BET, Fourier Transform Infrared Spektroskopi (FTIR), X-Ray Diffraction (XRD) dan Analisis gravimetrik terma (TGA). disintesis Zr / Ni / SBA-15 pemangkin diuji untuk CO2 pembaharuan metana. Tindak balas ini dianggap sebagai alternatif yang terbaik untuk menghasilkan gas sintesis kerana ia menggunakan dua gas rumah hijau yang banyak. CO2 pembaharuan hasil yang metana hidrogen yang rendah kepada karbon monoksida (/ CO H2) nisbah, yang adalah wajar untuk banyak proses sintesis industri. Sebaliknya, zirkonium dinaikkan pangkat spesies Nikel meningkatkan pembentukan pusat aktif untuk tindak balas. Akibatnya, pemangkin digalakkan dengan 1% berat daripada Zr melaksanakan dengan aktiviti pemangkin optimum dan menghasilkan jumlah yang lebih tinggi H2 pada suhu reaksi 800oC berbanding orang lain. Spesies zirkonium juga tersebar dan menggalakkan Nikel untuk terhad kepada liang-liang SBA-15. Dinding SBA-15 terhad pensinteran komponen Ni. Oleh itu, spesies Nikel tidak menjalani pensinteran kerana ia baik terbenam SBA-15 yang boleh menahan suhu yang lebih tinggi.

TABLE OF CONTENTS

LIST OF FIGURES

LIST OF TABLES

LIST OF ABBREVIATIONS

a	BET effective cross-sectional area
A	Pre-exponential factor
C	BET dimensionless constant
d	Interplane-distance of crystal
d_p	Catalyst particle diameter
d_t	Inner diameter of reactor
D	Crystalline size (Å)
$E\alpha$	Activation Energy
F	Molar Flowrate
k_{Sch}	Scherrer constant
m	BET solid mass catalyst
n	Order (integer)
n_i	Molar composition
N	Avogadro's constant (6.022×10^{23} mol^{-1})
P	BET partial vapour pressure/Partial Pressure
P_a	BET ambient pressure
P_o	BET saturated pressure
r	BET correlation coefficient
R	BET g.constant (8.314 E7 ergs/K.mol)/ universal gas constant (8.314 J/molK)
R^2	R-squared (measure of goodness of fit of regression)
$-r_A$	Rate of Reaction
r_k	BET Kelvin radius of pore
r_p	BET actual pore size
S	BET specific surface area
T	BET ambient temperature/Reaction temperature
t	time
V_a	BET volume of gas adsorbed at STP
V_{ads}	BET volume of N_2 adsorbed
V_{liq}	BET volume liquid
V_m	BET volume of gas adsorbed at STP to monolayer coverage
w	Weight fraction

wt%	Weight percentage
X	Conversion
Y_i	Yield
β_d	Angular width of half maximum intensity (degree/^{o})
γ	BET surface tension of N_2 (8.85 ergs.cm^{2}at 77.4 K)
Θ	Angle (degree/^{o})
λ	Wavelength (nm)
α	alpha
ρ	Density
K	Kelvin (temperature)
^{o}C	Degrees Celsius (temperature)
SBA-15	Santa Barbara Amorphous-15
XRD	X-Ray Diffraction
TGA	Thermo Gravimetric Analysis
BET	Brunauer, Emmett and Teller Surface Area Measurement
FTIR	Fourier Transform Infrared Spectroscopy
SEM	Scanning Electron Microscope

CHAPTER 1

INTRODUCTION

1.1 Background of the study

In recent years, considerable attention has been paid to global warming due to the greenhouse effect. The reduction and utilization of greenhouse gases such as carbon dioxide and methane is therefore becoming more and more important. In addition to the declining of crude oil reserves, the low natural gas prices coupled with discoveries of abundant shale gas reserves have replaced the depending on crude oil as energy supply with natural gas. According to BP Statistical Review of World Energy June 2015, the total world proved natural gas reserves is 187.1 trillion cubic meters whereas Malaysia contributes 1.1 trillion cubic meters *(BP Statistical Review of World Energy 2015).* However, the consumption is relatively small compared to the production rate which is subsequently leads to abundance of natural gas in storage. As the methane is the major component of natural gas (70-98%), many researches have been carried out with the catalytic methane reforming under different experimental conditions with different catalysts types as a way to valorize the natural gas to more valuable products by transforming it to syngas *(Ross, J. R. H., et al. 1996).* As a sequence of that, it is founded that suitable to be transformed through Fischer-Tropch and oxo-synthesis *(Albarazi et al. 2013).*

Technically, carbon dioxide can be used as a carbon source and the exhaust will be decreased as it is the most abundant waste produced by human activities. This is significant for the thrifty use of resources and the circulation economy *(Li, B., & Zhang, S. 2013)*. Thus, the carbon dioxide reforming of methane to produce syngas is considerably gain more attention in the past few years. The consumption of two major greenhouse gases (CO_2 and CH_4) by dry methane reforming and their conversion to syngas gives this process a great interest for environment protection and natural gas valorization *(Li, B., & Zhang, S. 2013).* Dry reforming of natural gas is a process where methane reacts with carbon dioxide in over a catalyst yielding

syngas with H_2/CO ratio of close to 1 *(Bentley, R. W. 2002).* Transformation of natural gas and CO_2 into valuable syngas by effective utilization of low-grade natural gas resources add on the advantages to the process. Therefore, the carbon dioxide reforming of methane is researched as a good route for producing high added value fuels such as hydrogen *(Liu et al. 2009).* But, there are some major drawbacks in this reaction should be well-balanced in order to increase the rate of profitability. The temperature needed for dry reforming reaction is higher than 800 ℃ to achieve acceptable conversions *(Wang et al., 1996).*

$$CO_2 + CH_4 \rightarrow 2CO + 2H_2 \qquad [\Delta H_{298} = 247 \text{ kJ/mol}]$$

This is an expensive process due to more energy is being consumed as the process is endothermic reaction (Tang et al. 2000). The main challenge of the industrial application of methane dry reforming is the development of active catalytic materials in order to optimize the catalytic activity and minimize the deactivation rate which is mainly due to sintering and coking.

This paper reports to synthesize Zirconium promoted Ni/SBA-15 catalyst for syngas production from CO_2 reforming of methane. On the other hand, the effect of different promoter loading on the Ni/SBA-15 catalyst was studied at normal reaction temperature. Using SBA-15 instead of any other support like carbon, alumina or pure silicate able to provide better stability to catalyst and also able to withstand the high temperature. The SBA-15 support with metallic catalyst possibly results in higher catalytic activity by resisting the sintering of metal species. Improving the properties of a catalyst by adding a promoter is most common technique in industries. In general, promoters can be categorized, according to their purpose which is facilitating the desired reaction or suppressing the unwanted processes. ZrO_2 have been known able to oxidize stored carbon. Furthermore, they are equipped for taking part in the catalytic reaction by oxidizing or diminishing reaction intermediates *(Dong, et al., 2002).* Zirconium, can store, discharge, and exchange oxygen species, which brings about an upgraded capacity to avoid carbon formation *(Dong, et al., 2002).* Dry reforming of natural gas is a process where methane reacts with carbon dioxide in over a catalyst and yield a syngas with H_2/CO ratio of close to 1. The advantages of this process are mitigation of CO_2 and natural gas, transformation of

natural gas and CO_2 into valuable syngas and effective utilization of low-grade natural gas resources consisting of natural gas and CO_2. The temperature needed for dry reforming reaction is higher than 800 ℃ to achieve acceptable conversions (Wang *et al.*, 1996). This is an expensive process due to more energy is being consumed as the process is endothermic. The main disadvantage of dry reforming is the significant production of coke, which are deposited on the surface of the catalyst as CO_2 is used as reagent in the process. This leads to the reduction in the activity of the reaction and also reduction of the useful life of the catalyst. The main challenge of the industrial application of methane dry reforming is the development of active catalytic materials as coke formation rate is high in dry reforming process. Therefore, the carbon dioxide reforming of methane is researched as a good route for producing high added value fuels such as hydrogen. But, there are some major drawbacks in this reaction should be well-balanced in order to increase the rate of profitability. This paper reports to investigate effect of different Zr-promoter Ni/SBA-15 catalyst for the CO_2 reforming of methane to syngas. The catalytic results obtained in this study were compared with those between previous researches related to this study.

1.2 Motivation

1. CO_2 reforming of methane reaction itself is an environmental friendly approach with utilization of two major greenhouse gases. Besides, the availability of raw material for the reaction also more promising.

2. Analysing the most suitable composition of promoter enable higher catalytic activity at specified temperature.

3. Using SBA-15 instead of any other support like carbon, alumina or pure silicate able to provide better stability to catalyst and also able to withstand the high temperature. The SBA-15 support with metallic catalyst possibly results in higher catalytic activity.

1.3 Problem Statement

Methane is the main ingredient in natural gas. However, the activation of methane remains difficult because of its strong C–H bond *(Dong, et al., 2002)*. The endothermic reaction requires high energy to decompose due to the presence of strong C-H bond between the molecules. CO_2 reforming of methane usually carried out at temperature range of 800ºC to 1000ºC to achieve considerably higher rate of conversion. Most of the previous studies are mainly related to higher catalytic activity accompanied by high temperature CO_2 reforming of methane. High reaction temperature of methane reforming causes sintering and high operating costs of process *(Lu Yao et al, 2015).* Another highly challenging problem is coke deposition on the catalyst. Performing the reforming at normal reaction temperature with SBA-15 support probably able to avoid these deactivation problems significantly. CO_2 reforming methane at normal reaction temperature parallel with high catalytic activity is new approach that attracted considerable attention in the past years. The highly potential CO_2 reforming methane is significant for the thrifty use of resources and the circulation economy. In this particular research, we conduct the study on Zirconium promoted Ni/SBA-15 catalyst that exhibits high activation ability. The effect of Zirconium promoter on the Ni/SBA-15 catalyst for the CO_2 reforming of CH_4 is to be further investigated.

1. 4 Objectives

The main objective of this literature is

1. To synthesize Zirconium promoted Ni/SBA-15 catalyst for syngas production from CO_2 reforming of methane.
2. To investigate the effect of Zirconium promoter on the Ni/SBA-15 catalyst at normal reaction temperature for CO_2 reforming of methane.

1.5 Scopes of study

The scope of this literature is as following;

1. To perform catalytic CO_2 reforming methane of synthesis gas using of Zirconium on the Ni/SBA-15 catalyst by varies the Zirconium loading (1, 3, 5, 7 wt%) as promoters in each system.

2. To study the Zirconium promoted Ni/SBA-15 catalyst performance in CO_2 reforming of methane in producing the best amounts of H_2 gas at normal reaction temperature of 800^oC.

3. To characterize the properties of catalyst using BET Surface Area Analysers, X-Ray Diffraction (XRD), Thermo Gravimetric Analysis (TGA), Fourier Transform Infrared Spectroscopy (FTIR Spectroscopy) and Scanning Electron Microscope (SEM).

CHAPTER 2

LITERATURE REVIEW

Overview

The dependence on fossil fuels as the main source of energy has caused serious energy crisis and environmental problems, such as fossil fuel depletion and emission of various pollutants. The increase in human population and the quality of life has resulted in the increase of demand for fuels, either for domestic or industrial purposes. In response to these issues, continuous efforts have been made to discover alternate fuel sources for sustainable development. One of the methods is to valorize natural gas in abundance into products of higher value and to solve the energy problem is to convert it into H_2. The use of H_2 as fuel offers an inexhaustible, efficient, and non-polluting alternatives because it offers an important reduction in NO_x, CO and CO_2 emissions *(John N. Armor., 1998).*

2.1 Properties of Synthesis Gas (Syngas)

Clean energy and alternative energy have become major areas of research worldwide for sustainable energy development. One of the most important research and development fields are on the syngas production and purification and also the usage of hydrogen as fuel cells. Hydrogen production has multiple application areas in chemical industry, food industry, and fuel cell systems. Due to the major advantages in efficiency and in environmental benefits, hydrogen energy in conjunction with fuel cells has attracted considerable attention in the global research community. H_2 production is a major issue in hydrogen energy development. Unlike the primary energy sources such as petroleum, coal, and natural gas, hydrogen energy is a form that must be produced first from the chemical transformation of other substances. Development of science and technology for hydrogen production is also important in the future for more efficient chemical processing and for producing ultraclean fuels. The development of H_2-based

and syngas-based energy systems require multifaceted studies on hydrogen sources, hydrogen production, hydrogen separation, hydrogen storage, H_2 utilization and fuel cells, H_2 sensor, and safety aspects, as well as infrastructure and technical standardization *(Song, 2010).*

The production and utilization of hydrogen energy is also associated with various energy resources, fuel cells, CO_2 emissions, and safety and infrastructure issues. Hydrogen energy and fuel cell development are closely related to the mitigation of CO_2 emissions. Fuel cells using hydrogen allow much more efficient electricity generation; thus, they can decrease CO_2 emission per unit amount of primary energy consumed or kilowatt per hour of electrical energy generated. Synthesis gas is formed by a variety of processes with sources ranging from commonly-used fossil fuels to completely renewable organic compounds. Synthesis gas basically consists of the following gases; H_2, H_2O, CO, CO_2, and CH_4 and can be used in many industrial applications such as the production of substitute natural gas, production of chemicals such as methanol, ethanol and ammonia, and it can also be made into liquid fuel for electricity generation *(Zohreh Ravaghi-Ardebili, 2014).*

Basically synthesis gas production can be done in so many ways, and in can be made from almost any carbon source ranging from natural gas to biomass, and oil products. Currently, natural gas is the most dominant feedstock and CH_4 reforming with CO_2 is the most preferred synthesis route in the industry in the production of syngas *(B. Fidalgo and J. A. Menéndez, 2013).* Moreover, the peak point for global gas production is researched to be slightly further than fossil fuels, it is found that mankind had probably used up half the gas needed to reach the world's resource limited conventional gas production peak *(R.W. Bentley, 2002).*

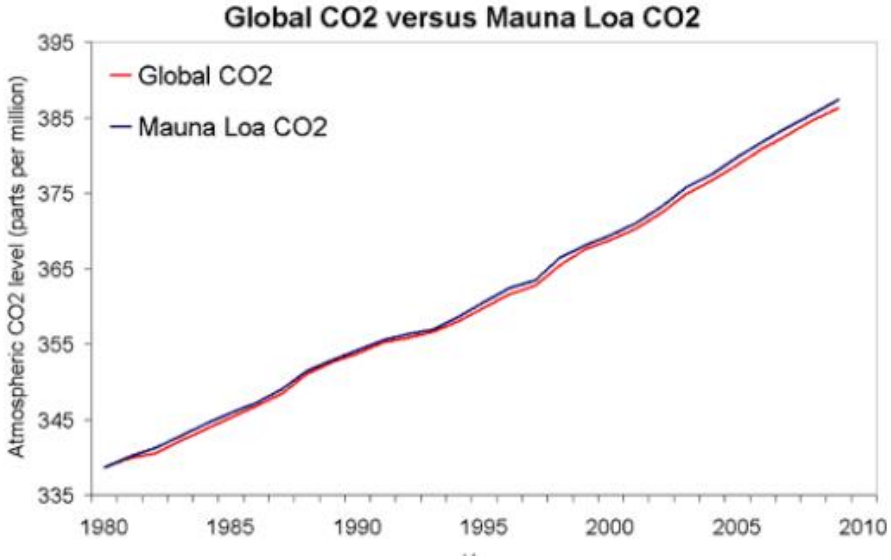

Figure 2.1 shows the global atmospheric CO_2 level in ppm from 1980 to 2010

In addition, climate change also presents itself as a risk we all should consider. According to BP Statistical Review 2015, the fossil fuel burning has released more than 277 billion tonnes of carbon to the atmosphere. Further emissions of carbon from coal combustions, and natural gas combustions account of more 6 million tonnes. Due to this, the CO_2 content in the atmosphere has been found to increase from 340 ppm in 1980 to 390 ppm in 2010 as shown in Figure 2.1 *(Skeptical Science, 2012).* Therefore research to produce syngas from alternate sources is a rather rational approach.

In an era where global warming is also a problem, H_2 has the potential to be an energy source which is non-polluting, inexhaustible, efficient, and somewhat cost attractive. Nevertheless, hydrogen produced from CO_2 reforming of CH_4 is the most preferred synthesis route in the industry in the production of syngas since it yields low hydrogen to carbon monoxide (H_2/CO) ratio *(Shaobin Wang, 1996).* As the reaction temperature is too high, low temperature CO_2 reforming of methane should have a considerable attention. On the other hand, this procedure has numerous attractive preferences over dry reforming: (i) Synthesis gas has a CO/CO_2 ratio without further, post-reformer reaction. (ii) The utilization of CO_2 implies that it is an appealing course toward CO_2 relief in stationary anthropogenic sources. (iii) It permits the conversion of methane, beforehand a waste part of oil stores, into a financially alluring feedstock *(Zhang, et al., 2003).*

2.2 Nickel (Ni) supported SBA-15 catalyst

Most normal metal oxide for methane reforming, for example, α- and γ-Al_2O_3, MgO, $MgAl_2O_4$, NiO, ZrO_2, TiO_2, CeO_2, La_2O_3, and CaO have been utilized as support materials. These supports have great porosity, which permits bigger surface region. Support assumes an urgent part since it focus the last molecule size of the metal, with its pore structure, morphology, and stage moves that it can experience. Moreover, a support can have a chemical part too, by initiating one or more reaction steps *(Liu, 2006).*

Among the catalysts analysed, Ni is one of a good replacement for noble metals, due to its comparable catalytic performance and low cost in terms of methane conversion and selectivity to synthesis gas. However, Ni based catalysts are more easily deactivated, because of carbon deposition and active metal species sintering and carbon deposition cannot be avoided over nickel-supported catalysts and for a CO/CO_2 molar ratio of unity *(Kroll, et al., 1996; Rostrup-Nielsen & Hansen, 1993)*. Ni-based catalysts are the most promising potential catalysts for the dry reforming of methane due to their high initial catalytic activity, low cost and extensive availability *(Chin J Catal, 2006).* However, at high reaction temperature, the thermal stability of the catalyst is reduced due to the coke formation on catalyst surfaces and the sintering of the Ni active sites *(Lu Yao et al, 2016).* Most common alternatives to overcome the drawbacks are addition of other components to Ni catalyst or changing the Ni-support interaction *(Ning Wang et al, 2013).* When the reaction is proceeded at low temperature these deactivation factor of catalyst can be reduced. From the past theory and experimental studies, it was affirmed that amount of Ni particles have a superior capacity to smother the carbon deposition *(Xu, et al., 2011).*

2.3 Santa Barbara Amorphous-15 (SBA-15)

A support with high surface area effectively increase Ni dispersion, and made the catalyst active and stable. Ordered mesoporous silicates have attracted a great deal of interest in the past decade because of their use in catalysis, separations, sensors, drug delivery, and optical devices. SBA- 15 was synthesized using tri-block copolymer poly (ethylene oxide) –poly (propylene oxide) –poly (ethylene oxide), which is commercially available as pluronics P123 ($EO_{20}PO_{70}EO_{20}$). SBA-15 possess large BET surface area (>700 m^2/g) with large pore diameter and large pore wall thickness. The large wall thickness results in higher hydrothermal stability than MCM-141 materials.

SBA-15 has proved to be very promising for the size selective separation of large biomolecules, because pore diameters are in the range required for these separations, and the silica framework is well suited for the development of bonded, selective sorption phases. It was reported that P123 never yielded monodisperse spheres, due to very strong hydrophobic forces that lead to a tendency to attain elongated cylindrical silicated-surfactant micelles. Parameters such as stirring rate, temperature, ionic strength, pH, and reactant composition can influence the morphology of SBA-15 particles. Mesoporous silica of Santa Barbara Amorphous-15 (SBA-15) with high specific surface area (up to 1160 m^2/g), high hydrothermal stability, well-ordered hexagonal structure with tunable pore size (47-300 Å), thick wall (31-64 Å) and large pore volume (up to 2.5 cm^3/g), has great potential in many areas of chemistry and material science *(Baitao Li and Shuyi Zhang, 2013).* The ordered mesoporous structure enable Ni particles to be confined in the channels of the mesoporous material *(Chin J Catal, 2006).*

2.4 Zirconium Promoter

Zirconium Oxide (ZrO_2) have been known able to oxidize stored carbon. Further, they are equipped for taking part in the catalytic reaction by oxidizing or diminishing reaction intermediates. *Dong et al.* considered methane reforming over $Ni/Ce_{0.15}Zr_{0.85}O_2$ catalysts. They concluded that there were two sorts of active sites that exist, one for methane activation and one for steam or oxygen activation. Zirconia, can store, discharge, and exchange oxygen species, which brings about an upgraded capacity to avoid carbon formation *(Dong, et al., 2002).* Improving the properties of a catalyst by adding a promoter is most common technique in industries. In general, promoters can be categorized, according to their purpose which is facilitating the desired reaction or suppressing the unwanted processes. In this case, Zirconium is used as promoter to increasing the activity of the catalyst. For the CO_2 reforming of methane, Zirconium was found to enhance the dispersion of Nickel species *(Baitao Li and Shuyi Zhang, 2013).* Simply, the promoters can create more active sites at low temperature, influence the electronic structure of the active phase *(Gary Jacobs, 2002).*

2.5 Sol-gel Method

Crucially, the preparation procedure also possess strong influence on the catalyst textural, structural and chemical features *(Baitao Li and Shuyi Zhang, 2013).* Hydrothermal method is the most common approach for the introduction of the active metal into the ordered mesoporous silica. However, controlling the stoichiometric composition of product is quite difficult using this method. This is mainly due to the addition of the metal ion precursor system before the hydrothermal treatment and some metal ions exist in synthesis solution. The filtration process after the treatment causes loss of the metal content. In recent days, sol-gel method is considered to be the best alternative since it has the advantages of controlling stoichiometric composition and shape of target product *(Baitao Li and Shuyi Zhang, 2013).*

Sol-gel is broadly defined as the preparation of a sol, and removal of solvent. The sol can be produced from inorganic or organic precursors. Sols and gels are two forms of matter that have been known to exist naturally for a long time. The first step of any sol-gel process always consists in selecting the precursors of the wanted material. It is that

precursor that lead to the reaction towards the formation of either particles or polymeric gels. The colloidal particles obtained can then be precipitated and treated according to one of the conventional processing technique such as cold pressing, hot pressing and sintering in order to produce the desired ceramic. The colloidal particles can also be dispersed into a stable sol before being transformed into a gel. Sols and gels can also be spinned into fibers or transformed trough one of other various techniques into a coating material. If a gel powder for melting purposes is required, then the gel may be dried and no special cares need to be given to fracturation *(Alain C. Pierre, 2002).* On the other hand, controlled gelatin and drying lead to the formation of mono-sized droplets which can reach several hundred micrometers in diameter. Figure 2.2 shows a simplified chart of sol-gel processing as discussed.

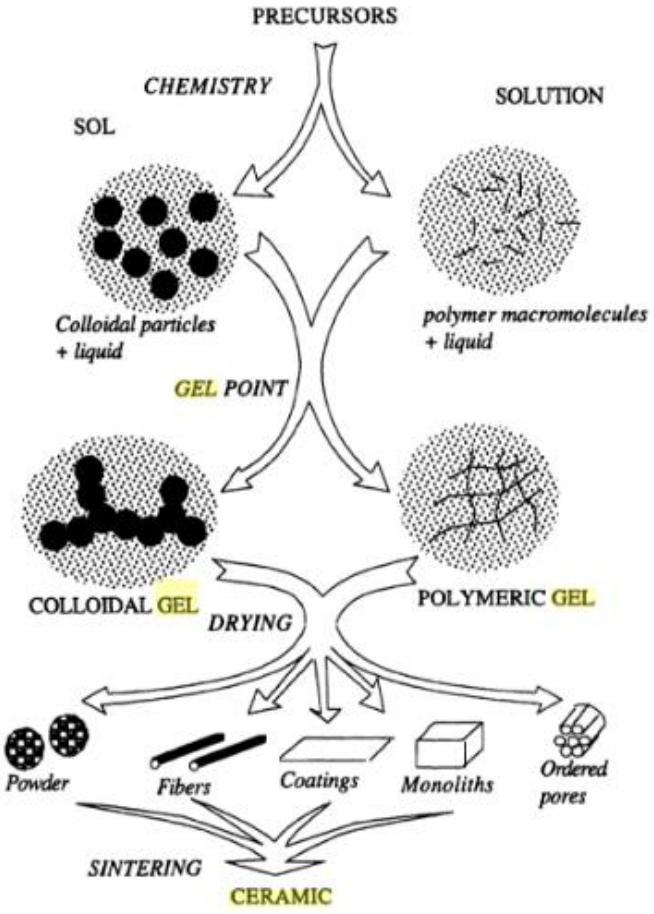

Figure 2.2 shows a simplified chart of sol-gel processing.

CHAPTER 3

MATERIALS AND METHODS

Chapter Overview

This chapter basically covers the materials and its usage in the catalyst preparation and the CO_2 reforming of methane reaction. Besides that, the methodologies of the preparation of Zr-Ni/SBA-15 as the catalyst are extensively outlined. The methodology of the CO_2 reforming of methane reaction to produce syngas is also outlined. This chapter also covers the physicochemical analysis to be done on the fresh catalyst such as BET Surface Area Analysers, X-Ray Diffraction (XRD), Thermo Gravimetric Analysis (TGA), Fourier Transform Infrared Spectroscopy (FTIR Spectroscopy) and Scanning Electron Microscope (SEM).

3.1 Materials

The table 3.1 shows the list of chemical components used in this research. Materials such as Nickel (II) nitrate hexahydrate ($Ni(NO_3)_2.6H_2O$), Zirconium (IV) oxide (ZrO_2), triblock copolymer Pluronic P123 ($EO_{20}PO_{70}EO_{20}$) and Tetraethylorthosilicate (TEOS) purchased from Sigma Aldrich Malaysia at high purity. Even though the purpose of this project is for reduce the greenhouse gases, at an experimental basis, Carbon dioxide (CO_2) feedstock with highest purity (>99.99%) used in the reaction is purchased together with methane gas (CH_4).

Table 3.1: Properties of materials used and their applications

No	Material	Purity (%)	Application
1	Nickel (II) nitrate hexahydrate	99.99	Preparation of catalyst
2	Zirconium (IV) Oxide	≥ 97.00	Preparation of catalyst [Promoter]
3	Ethanol	≥99.5	Preparation of catalyst
4	Hydrochloric Acid (HCl)	≥99.0	Preparation of catalyst
5	Triblock Copolymer Pluronic (P123)	≥99.0	Preparation of catalyst [Support]
6	Tetraethylorthosilicate (TEOS)	≥99.0	Preparation of catalyst [Support]
7	Methane Gas	≥99.0	Catalyst Testing
8	Carbon dioxide Gas	≥99.8	Catalyst Testing

3.2 Preparation of Zr-Ni/SBA-15 Catalyst

The chemicals used in this study were at the analytical reagent grade without further purification. The Zirconium (Zr) promoted Ni/SBA-15 synthesized using the sol-gel method. Specifically, triblock copolymer Pluronic P123 ($EO_{20}PO_{70}EO_{20}$) was used as the structure directing agent and Tetraethylorthosilicate (TEOS) as the silica support source for the catalyst *(Li, B., & Zhang, S. 2013).* An adequate amount of P123 dispersed in TEOS under vigorous stirring at 60^{o}C for 10 minutes to obtain a homogeneous solution. The ethanol solution containing a requisite amount metal precursor solutions, $Ni(NO_3)_2$ and ZrO_2 corresponding to different Zr to Ni/SBA-15 molar ratio added to the above solution under constant stirring at 60^{o}C for another 10 minutes. After the solution cooled down to the room temperature, 2.0 ml hydrochloric acid added the mixture under constant stirring for 2 hours. After stored at room temperature for 24 hours, the light green gel formed, and it is transferred into an oven of 110^{o}C and drying process continued for 4 hours *(Li, B., & Zhang, S. 2013).* Finally, the pre-dried sample calcined in a muffle furnace at 800°C for 5 hours in air, yielding respectively the Zr-Ni/SBA-15 catalyst *(Li, B., & Zhang, S. 2013).* The products denoted as x-Zr-Ni/SBA-15, where "x" indicates the molar ratio of Zr to Ni/SBA-15.

3.3 Catalyst Characterization

Analysis was done to evaluate both formed catalyst using certain instruments for reaction study. Catalyst characterization is important in catalyst design as it enables the study of the catalyst's chemical & physical properties and their effects in reaction kinetics under various conditions. The following are the instruments used in the catalyst characterization part.

3.3.1 X-Ray Diffraction

X-ray diffractometer (XRD) is an instrumental technique which involves phase identification, and quantitative and qualitative analysis of materials. It is based on the interference of monochromatic x-rays and crystalline sample. Figure 3.1 shows the schematic of XRD. The generated rays were initially generated by a cathode ray tube (F), and the x-rays will be filtered to produce monochromatic radiation (SS1) aligned and concentrated towards the sample (S). The interference produced (SS2) were corresponded to Bragg's Law (Equation 3.1). After detecting (AS) the diffracted x-rays, the sample was scanned through a range of 2θ angles to identify all possible diffraction directions of the sample's crystal lattice structure.

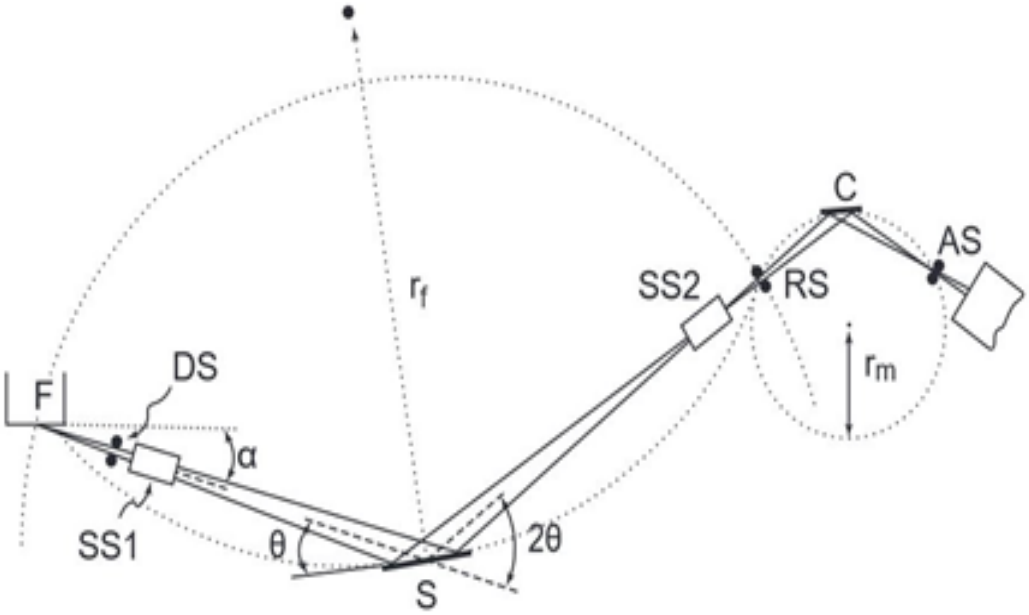

Figure 3.1: Bragg-Brentano parafocusing geometry *(Cullity & Stock., 2001)*

The mean crystallite size can be calculated via the Scherrer equation (Equation 3.1)

$$D = \frac{k_{Sch}\lambda}{\beta_d cos\theta} \qquad (3.1)$$

Where D is the crystallite size (Å),

k_{Sch} is the Scherrer constant,

λ is the wavelength is x-ray,

β_d is the angular width if half-maximum intensity (degree)

θ is Bragg's angle (degree).

In current research, the samples were irridated by Ni-filtered CuKα with a wavelength of 1.542 Å at 40mA and 45kV and scanning was done from 10ºC (283K) to 80ºC (353K) at 4 min^{-1}. The XRD equipment that was used was Rigaku Miniflex II.

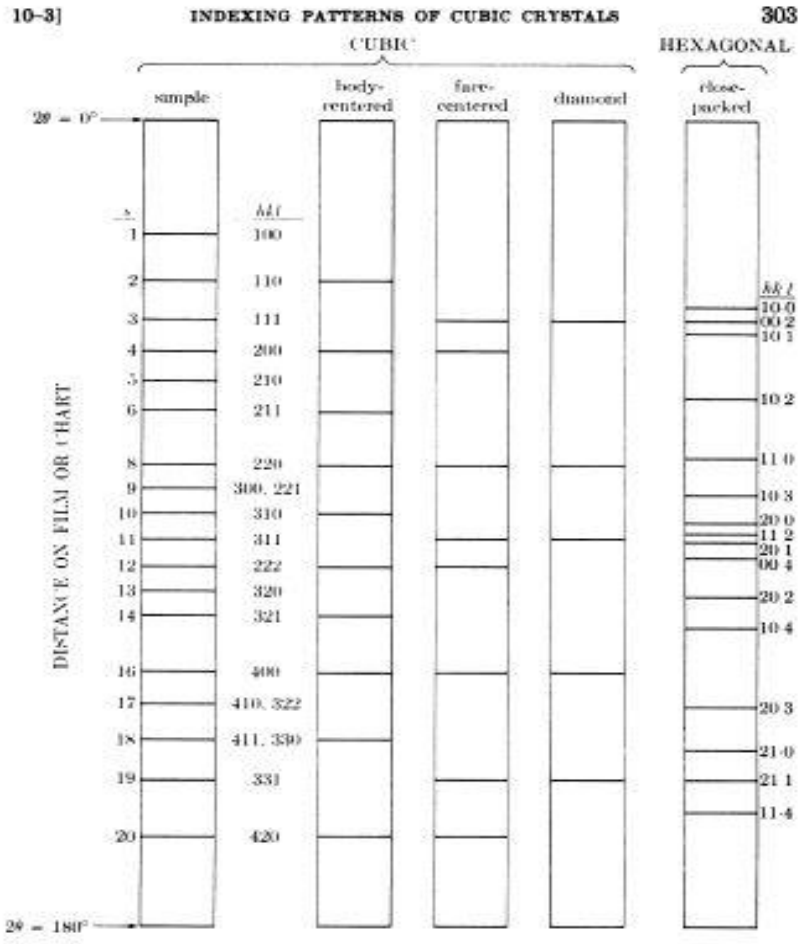

Figure 3.2: Calculated diffraction patterns for various lattices *(Cullity & Stock., 2001)*

The crystalline structure of the catalyst may be determined by the following method. Each of the four common cubic lattices types is recognizable by their characteristic sequence of diffraction lines, and these in turn are explained by their sequential s values.

For simplicity, the sequences are explained in the Figure 3.2.

Simple cubic: 1, 2, 3, 4, 5, 6, 8, 9, 10, 11, 12, 13, 14, 16,...

Body-centered cubic: 2, 4, 6, 8, 10, 12, 14, 16,...

Face-centered cubic: 3, 4, 8, 11, 12, 16,...

Diamond cubic: 3, 8, 11, 16,....

3.3.2 Thermogravimetric Analysis (TGA)

The basic concept of TGA is determining the differential mass of catalyst system when oxidised or reduced using oxygen of hydrogen respectively. Any decrease in sample mass is due to the release of by-products such as nitrates and water in the reaction due to decomposition of metal nitrate precursor of uncalcined solid catalyst sample. This must be carried out in a Q500-series model TGA unit. For each analysis, the 2 catalyst types will be ramped up at 10,15 and 20 K min-1 to 1173 K and held for 1 hour under 50 ml min-1 of high purity air. Thermogravimetric Analysis functions on a fundamental set of principles which are as follows;

i. The trend in change of the mass of the sample is studied while the sample is subjected to a controlled temperature program.
ii. The temperature program is most probably linear with temperature. Nevertheless, isothermal studies can also be carried out when the change in sample mass with temperature are constant.
iii. TGA is inherently quantitative, and therefore an extremely powerful thermal technique, but it gives no direct chemical information.

Table 3.2 depicts the various processes that lead to mass gain or loss in TGA runs**.**

Process	Weight gain	Weight loss
Adsorption	●	
Absorption		●
Desorption/Drying		●
Dehydration/desolation		●
Sublimation		●
Vaporization		●
Decomposition		●
Solid-solid reactions		●
Solid gas reactions	●	●
Magnetic transitions	●	●

3.3.3 BET Surface Measurement

Brunauer-Emmett-Teller method *(Brunauer et al., 1938)*, which is an extension of Langmuir's pioneer work *(Langmuir, 1916)* regarding the study of monomolecular adsorption is widely used in this work. The specific surface area of the sample was determined by physical adsorption of gas onto the surface of the solid which will correspond to a monomolecular layer on the surface. In this research, N_2 was used as the adsorbate which has a boiling point of 77.4K. The equations associated with BET are as follows;

$$\frac{1}{[V_a\left(\frac{P_o}{P}-1\right)]} = \frac{C-1}{V_m C} \times \frac{P}{P_o} + \frac{1}{V_m C} \qquad (3.2)$$

Where,

P = Partial vapour pressure of adsorbate gas in equilibrium with the surface at 77.4K

P_o = Saturated pressure of adsorbate gas

V_a = Volume of gas adsorbed at standard temperature and pressure (STP)

V_m = Volume of gas adsorbed at STP to monolayer coverage

C = Dimensionless constant of adsorbate

V_a was measured at each of not less than the three values of P/P_o. After all parameters were determined, the BET values were plotted against P/P_o relative to Equation (3.2). A straight line plot relative to the approximate pressure range of 0.05 to 0.3 with an acceptable linear regression of not less than 0.9975 would give a precise value for the following parameter;

$$Intercept = \frac{1}{V_m C} \qquad (3.3)$$

$$V_m = \frac{1}{(Slope + Intercept)} \qquad (3.4)$$

$$C = \left(\frac{Slope}{Intercept}\right) + 1 \qquad (3.5)$$

Then, the specific surface area can be calculated from Equation (3.6);

$$S = \frac{V_m N a}{m \times 22400} \qquad (3.6)$$

where

N = Avogadro's constant (6.022 x 1023 mol^{-1})

a = Effective cross sectional area of one adsorbate molecule

m = Mass of solid catalyst

With the assumption that all the pores are filled with liquid N_2, the total pore volume was derived from the amount of vapour adsorbed at a relative pressure which is close to unity. Apart from that, if the pore width is more than 50nm, the solid material is assumed to have no macropores and the isotherm will remain nearly horizontal over a range of P/P_o near to unity and the pore volume becomes well defined. If the isotherms rise rapidly near P/P_o close to 1 for mesopores, the limiting adsorption may be identified with the total pore volume. The volume of N_2 adsorbed V_{ads} can be converted to the volume of the liquid N_2 (V_{liq}) contained in the pores. This conversion is depicted by the following formula (Equation 3.7)

$$V_{liq} = \frac{P_a V_{ads} V_m}{RT} \qquad (3.7)$$

where

P_a = Ambient pressure

T = Ambient temperature

V_m = Molar volume of the liquid N_2 (34.7 $cm^3.mol^{-1}$)

Since pores which are not filled below a P/P_o of 1 have a negligible effect or contribution to the total pore volume, the average pore size can be estimated from pore volume. Pore size distribution which is the distribution of pore volume with respect to pore size can be configured. Thermo-Scientific Surfer possess the ability to perform calculation on the pore size distribution for both branches of isotherms. Mesopore size calculations were executed by assuming cylindrical pore geometry using Kelvin equation *(Gregg & Sing, 1982)*;

$$r_k = \frac{-2\,V_m\gamma}{RT\ln\left(\frac{P}{P_o}\right)} \qquad (3.8)$$

where

γ = The surface tension of N_2 at its boiling point (8.85 ergs.cm^2 at 77.4 K)

V_m = Molar volume of liquid N_2 (34.7 cm^3 mol^{-1})

R = Gas constant (8.314 E^7 ergs/K.mol)

T = N_2 boiling point (77.4K)

P/P_o = Relative pressure of N_2

R_k = Kelvin radius of pore

With the integration of appropriate constants of N_2, Equation (3.8) can be reduced to Equation (3.9)

$$r_k = \frac{4.15}{\log(P/P_o)} \qquad (3.9)$$

The Kelvin radius is defined as the radius of the pore in which condensation occurs at P/P_o. However, it must be noted that r_k does not represent the actual pore radius because some adsorption had taken place before condensation on the walls of the pores. Besides that, there is a high chance that an adsorbed layer might have remained on the walls when evaporation occurred during desorption. Therefore, the actual pore radius can be given by the following equation;

$$r_p = r_k + t \qquad (3.10)$$

where

t = Thickness of adsorbed layer.

The t value was estimated by utilizing an equation proposed by *(De Boer et al., 1966)* represented as equation 3.11 in this literature.

$$t = \left[\frac{13.99}{\log\left(\frac{P}{P_o}\right) + 0.034}\right]^{0.5} \qquad (3.11)$$

Computations made in Thermo-Scientific Surfer in the finding out the pore size distribution based on the methods proposed by Barrett, Joyner, and Halenda *(Barrett et al., 1951)* as it is more popular and widely used for the computation of the pore size distribution. As recommended by *(Barrett et al., 1951)*, procedures are based on the emptying of the pores by a step-wise reduction of P/P_o and the derived pore size distribution is expressed in graphical form of $(\delta V_p/\delta r_p)$ versus r_p or d_p. For this research, Liquid N_2 with a cross-sectional area of 0.162 nm^2 will be used for BET surface area measurement on sample. The adsorption/desorption cycles will be performed at 77 K in a Thermo-Scientific Surfer unit.

3.3.4 Fourier Transform Infrared Spectroscopy (FTIR)

Fourier Transform Infrared Spectroscopy, also known as FTIR Analysis or FTIR Spectroscopy, is an analytical technique used to identify organic, polymeric, and in some cases, inorganic materials. The FTIR analysis method uses infrared light to scan test samples and observe chemical properties. The first step is to collect a background spectra to subtract from the test spectra to ensure the actual sample is all that is analyzed. Next, the sample is analyzed by LTI's fully-computerized Fourier Transform Infrared Spectroscopy system which generates the absorbance spectra showing the unique chemical bonds and the molecular structure of the sample material. This profile is in the form of an absorption spectrum which shows peaks representing components in higher concentration. Absorbance peaks on the spectrum indicate functional groups (e.g. alkanes, ketones, acid chlorizes). Different types of bonds, and thus different functional groups, absorb infrared of different wavelengths. Although the analysis is performed in absorbance, it can be radiation converted to transmittance, since they are simply the inversions of each other. The analytical spectrum is then compared in a reference library program with cataloged spectra to identify components or to find a "best match" for unknown material using the cataloged spectra for known materials.

3.4 CO_2 Reforming of Methane

The framework for multifunctional catalytic reactor system illustrated in schematic diagram below.

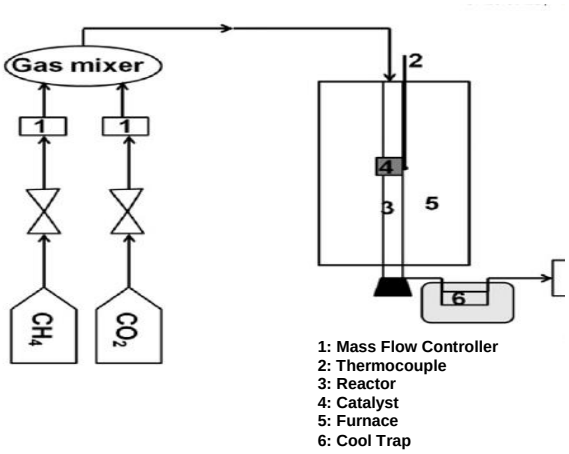

Figure 3.3: Simplified experiment set up for CO_2 reforming of methane. Modified from *L. Yao et al. (2016)*

The experiment was conducted in lab scale fixed bed quartz reactor. The powder catalyst were palletized using 26mm sieve tray in order to imitate real industrial operating condition. Palletized catalyst able to retain the amount of catalyst in the reactor. All the CO_2 reforming of methane reactions were conducted in a stainless steel fixed bed reactor which is placed in a furnace. In order to prevent back-mixing flow back arrester installed along the pipeline. In the CO_2 reforming of methane reaction, the reactor was prepared for the reaction by inserting approximately 0.2g catalyst into a steel tube. Quartz wool was used as a bed for the catalyst on a stainless steel support inside the reactor. The spread of the catalyst was ensured to be even throughout the inner diameter of the reactor. Then, the reactor was clamped into the furnace. The reactor was placed carefully in such a way that the thermocouple will be touching the middle of the reactor, where the catalyst is located. The furnace door was closed and the gaps will be sealed to prevent heat loss. The leak test performed using inert gas (N_2) and liquid leak detector before turning on any gaseous reactants (CH_4 and CO_2).

One of the crucial step conducted before conducting the CO_2 reforming of methane is pre-treatment. Since the metallic component Ni is used as the catalyst, the pre-treatment was conducted at 700^oC for 1 hour. The experiment will be set up as shown in Figure 3.3. CO_2 reforming of methane will be conducted in inert atmospheric pressure. The flowrate of CO_2 to methane was fixed at 1:1. The temperature of the

furnace fixed at 800°C. The outlet flow rate was measured every 30 minutes using a bubble meter and gas samples was collected. Formula for estimating gas flow rate is shown as in equation below:

$$\text{Flow fate (ml min}^{-1}) = \frac{20 \text{ ml}}{\text{Time required for flowing bubble from 0 to 20 ml (s)}} \times \frac{60 \text{ s}}{1 \text{min}}$$

The gas collected at the end of the reactor will be analysed using gas chromatography (GC). The findings will be discussed in the result presentation and reports.

CHAPTER 4

RESULTS AND DISCUSSIONS

Chapter Overview

This chapter details out the results and discussions of the CO2 reforming of methane using Zr-promoted Ni/SBA-15 as catalyst with different promoter content. Fresh catalyst characterization will be discussed using established techniques such as BET Surface Area Analysis, X-Ray Diffraction (XRD), Fourier Transform Infrared Spectroscopy (FTIR) and Thermal Gravimetric Analysis (TGA). The reaction study will be outlined where the yields, conversions and the H_2/CO ratios will be evaluated.

1.1 Fresh Catalyst Characterisation

4.1.1 Brunauer-Emmett-Teller (BET) Analysis

The Brunauer-Emmett-Teller (BET) specific surface area of Zr-promoted Ni/SBA-15 was obtained from the results of N_2 adsorption/desorption measurements at 77 K using Thermo-Scientific Surfer. Figure 4.1 (a), (b), (c) and (d) shows the adsorption and desorption isotherms for the researched catalyst samples. Based on the isotherm data, the surface area, pore volume and pore diameter were determined with the equations covered in Chapter 3.

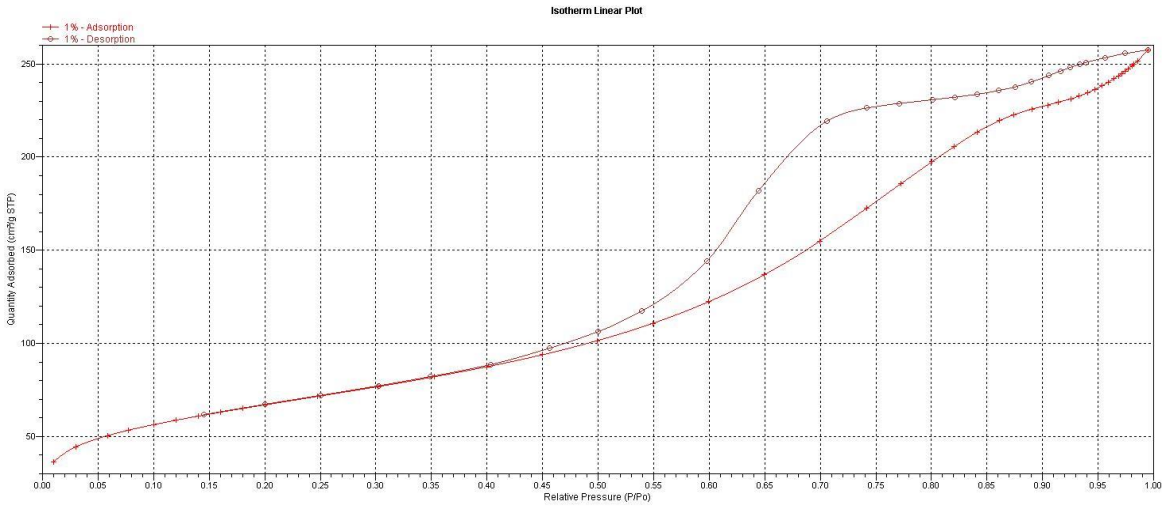

Figure 4.1 (a) shows the adsorption/desorption isotherms for 1wt% of Zr-Ni/SBA-15

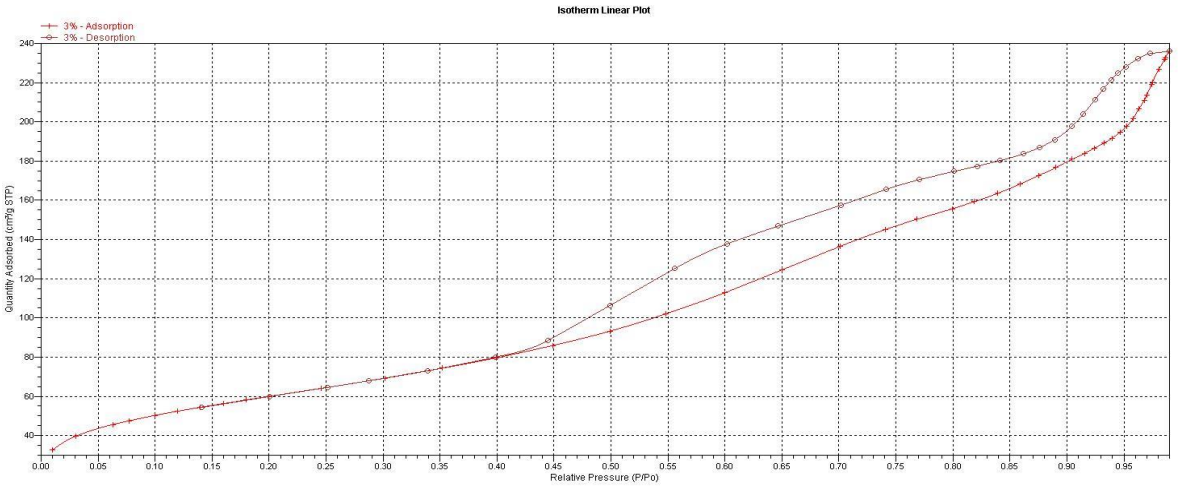

Figure 4.1 (b) shows the adsorption/desorption isotherms for 3wt% of Zr-Ni/SBA-15

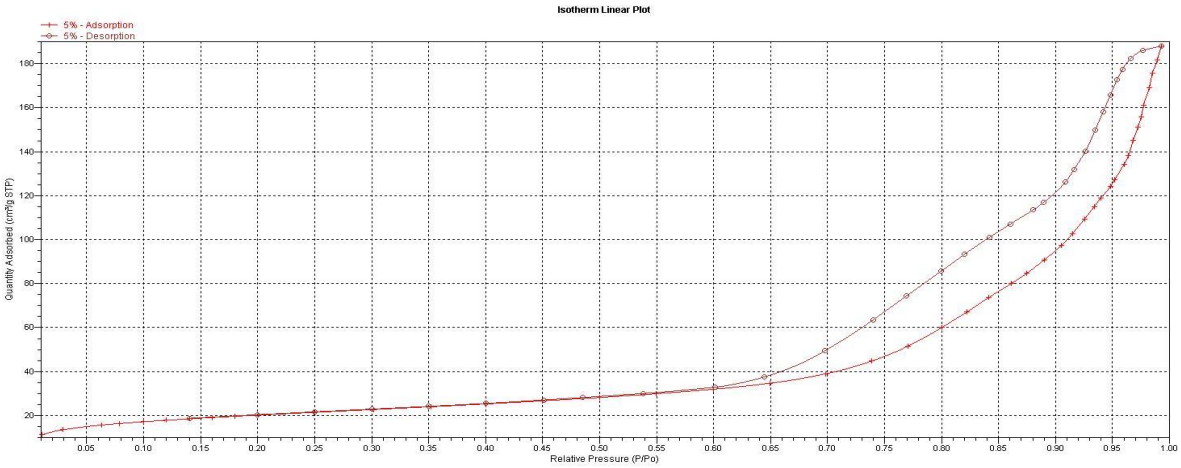

Figure 4.1 (c) shows the adsorption/desorption isotherms for 5wt% of Zr-Ni/SBA-15

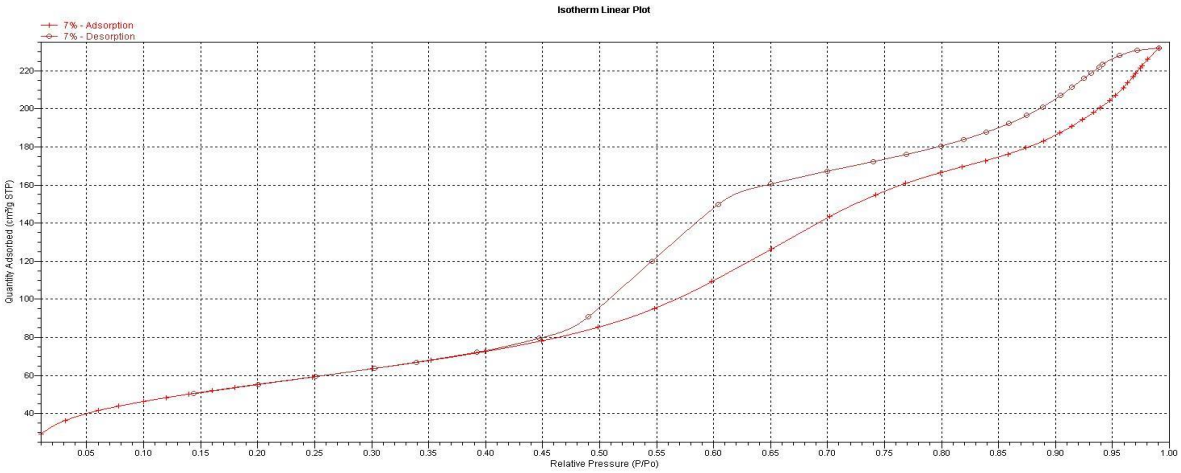

Figure 4.1 (d) shows the adsorption/desorption isotherms for 7wt% of Zr-Ni/SBA-15

Based on the isotherm data, the surface area, pore volume and pore diameter were determined. Table 4.1 summarizes the BET surface area and pore volume and pore diameter of the researched catalyst along with some comparisons. The BET specific surface area was analyzed using the BET method while the pore volumes and average pore diameters were computed by BJH method which analysis result was available along with the BET test results.

Table 4.1: BET surface area and pore volume and pore diameter of catalyst samples

Catalyst	BET specific surface area, A_{BET} (m^2/g)	Pore volume, *V*p (cm^3/g)	Average pore diameter, *D*p (Å)
1wt% Zr-Ni/SBA-15	240.0202	0.411027 (Adsorption) 0.407965 (Desorption)	61.228 (Adsorption) 52.891 (Desorption)
3wt% Zr -Ni/SBA-15	216.8302	0.378177 (Adsorption) 0.375335 (Desorption)	62.448 (Adsorption) 54.760 (Desorption)
5wt% Zr-Ni/SBA-15	70.7785	0.293035 (Adsorption) 0.292238 (Desorption)	155.554 (Adsorption) 124.741 (Desorption)
7wt% Zr-Ni/SBA-15	199.3480	0.368307 (Adsorption) 0.366349 (Desorption)	63.138 (Adsorption) 54.062 (Desorption)
SBA-15 *(ZHANG Meili et al, 2006)*	630.9	0.92	78.3
Ni/SBA-15 *(ZHANG Meili et al, 2006)*	474.5	0.68	66.6 (Adsorption) 38.9 (Desorption)

For the catalyst with 12.5wt% Nickel, the BET specific surface area decrease as the as the Zirconium loading increases due to pore blockage. According to the results, it is apparent that the increase in Zirconium weight percentage led to decrease in specific surface area and pore volume. The decrease pore volume for the catalyst samples indicates the Zirconium species embedded into mesoporous instead of Nickel. The average pore diameter obtained from the BET isotherm shows similar results with previous research *(ZHANG Meili et al, 2006).* The smaller surface area is evidence that the type of SBA-15 used for the catalyst impregnation consisted of mainly alpha (α) particles rather than beta or gamma particles. Alpha type particles were chosen during catalyst preparation because of its stability. Apart from that, the prospects of using alpha particles were also taken into investigations because the same catalyst created using gamma (γ) particles were found to have smaller pore diameters and larger surface areas *(Siew et al.,2014).*

4.1.2 X-Ray Diffraction (XRD) Analysis

X-Ray Diffraction was employed for phase identification in terms of qualitative and quantitative analysis on the fresh catalyst sample. The XRD analysis was done using the MiniFlex II with the notation of determining the catalyst's crystalline phase. Figure 4.2 shows the complete pattern from a range 2θ angles (10° to 80°) to identify all the possible diffraction directions of crystal lattice structure for the catalyst samples.

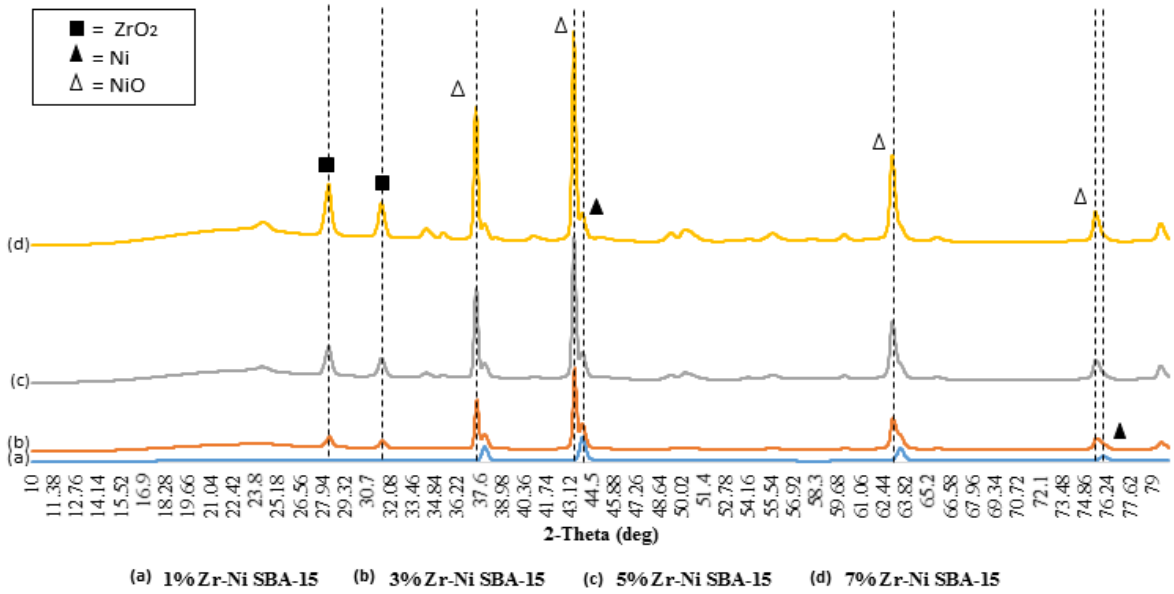

Figure 4.2 XRD analysis for catalyst samples with different Zr loadings.

Figure 4.2 shows the complete XRD patterns of the catalyst samples with different Zr loadings. The broad diffraction peaks at 2θ = 23° indicates the amorphous nature of SBA-15 *(Dao et al. 2008).* The characteristic peaks for NiO species at 2θ = 37.2°, 43.1°, 62.8° and 75.4°, corresponding respectively to the planes (1 1 1), (2 0 0), (2 2 0) and (3 1 1) of cubic NiO species (JCPDS 65-5745) were observed for all the calcined samples except for the 1wt% Ni/SBA-15 catalyst *(Cullity et al. 2001).* The NiO particles have a preferential orientation along the (2 0 0) plane, since the intensity of peak has the highest value. Hence, the crystallite sizes of the particles were determined using the diffraction peak of (2 0 0) NiO plane. The diffraction peaks of metal Ni at 44.4° and 76.4° assigned to (1 1 1) and (2 2 0) planes respectively of (JCPDS 04-0850) *(Chin J Catal, 2006).* Ni species diffraction peaks were observed for all the samples prepared. On the other hand, Zr was not detected at 1wt% catalyst due to small amount of Zr. This shows Zirconium was well dispersed and well impregnated on the catalyst.

While for the other samples, the existence of the ZrO_2 phase in the samples is at a very small level. ZrO_2 is shown by two main peaks at diffraction angles of 28.21° and 31.45° from crystals planes of (1 1 1) and (1 1 1) respectively *(Yao, Lu, et al.2016).* This results indicates the sample with 1wt% of zirconium is well dispersed and promote the Ni species to be confined to the pores of SBA-15 with some size scope limitation.

Using Scherrer's Equation, the calculated crystallite sizes of particles are shown in Table 1 below. The position of all the diffraction lines on the chart of the length which is characterized by a pair of lines, followed by a single line, followed by a pair, another single line suggests that the crystal structure of the catalyst follows a face-centered cubic pattern (FCC).

Table 4.2 shows the calculated crystalite sizes of catalyst particles

Catalyst Samples	**d_{NiO} (nm)**	**d_{Ni} (nm)**	**FWHM (deg)**
1wt% Ni/SBA-15	-	22.4172	0.377
3wt% Ni/SBA-15	49.2386	-	0.199
5wt% Ni/SBA-15	47.7021	-	0.176
7wt% Ni/SBA-15	46.1499	-	0.183

- $d_{NiO} = (0.89\lambda)(\beta \cos \theta)$

Therefore, the Ni particles increase in size as the percentage of promoter increase. The relatively large promoted species, might be confined to the pores instead of the Ni species. 1wt% of Zirconium provides better dispersion to the Ni species. From the Scherrer's Equation, the crystalline size of Ni is found to have an average of 22.4 nm at 43.9°.

4.1.3 Thermogravimetric Analysis (TGA) Analysis

Investigations of gas-solid catalyst interactions were carried out to report the thermal calcination profiles of Zr-promoted Ni/SBA-15 catalyst with different Zirconium loadings. The calcination profiles were obtained from a Q500-series model Thermogravimetric Analyzer unit under an air blanket. Figure 4.3 (a), (b), (c) and (d) illustrates the thermogram of the researched catalyst samples with changes of weight against temperature.

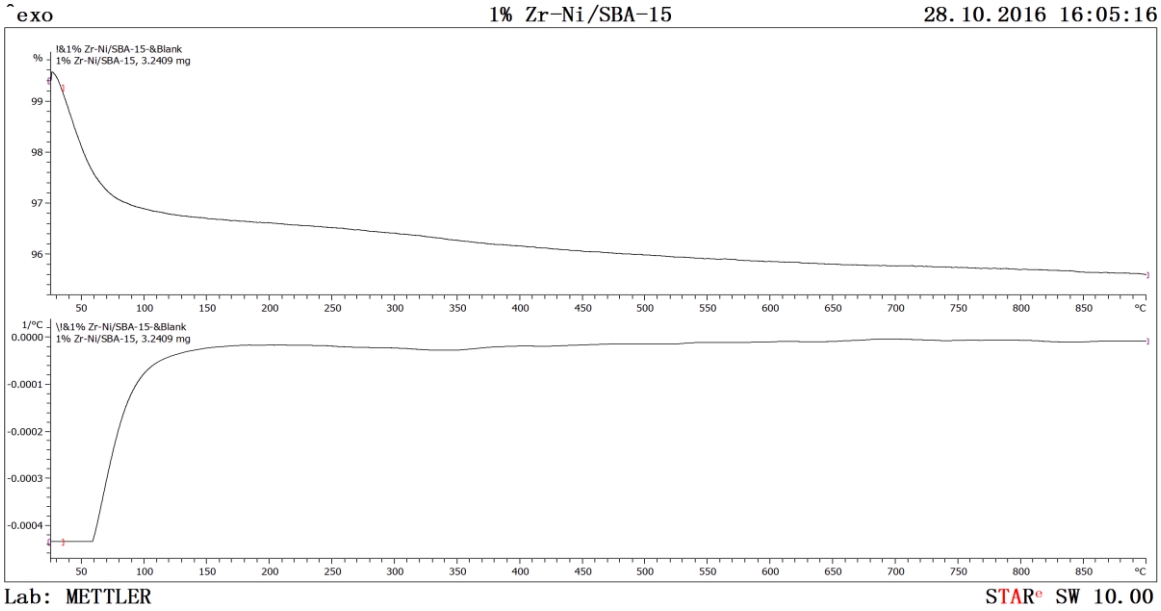

Figure 4.3 (a) shows thermogram profile for 1wt% Zr-promoted Ni/SBA-15 catalyst

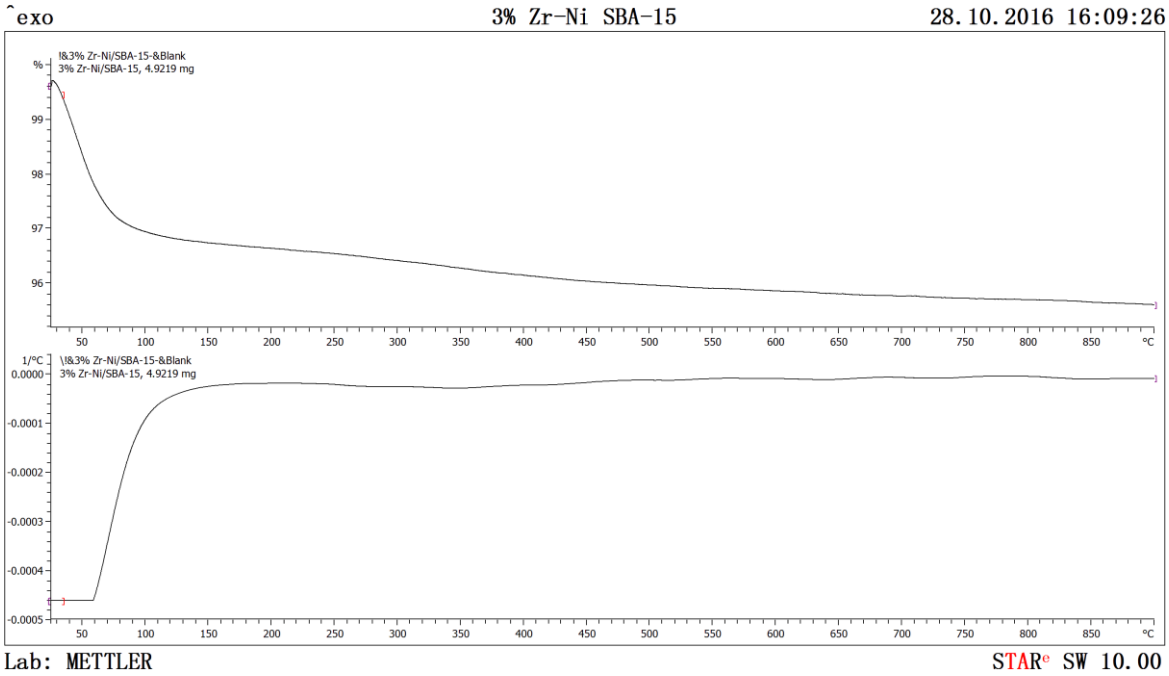

Figure 4.3 (b) shows thermogram profile for 3wt% Zr-promoted Ni/SBA-15 catalyst

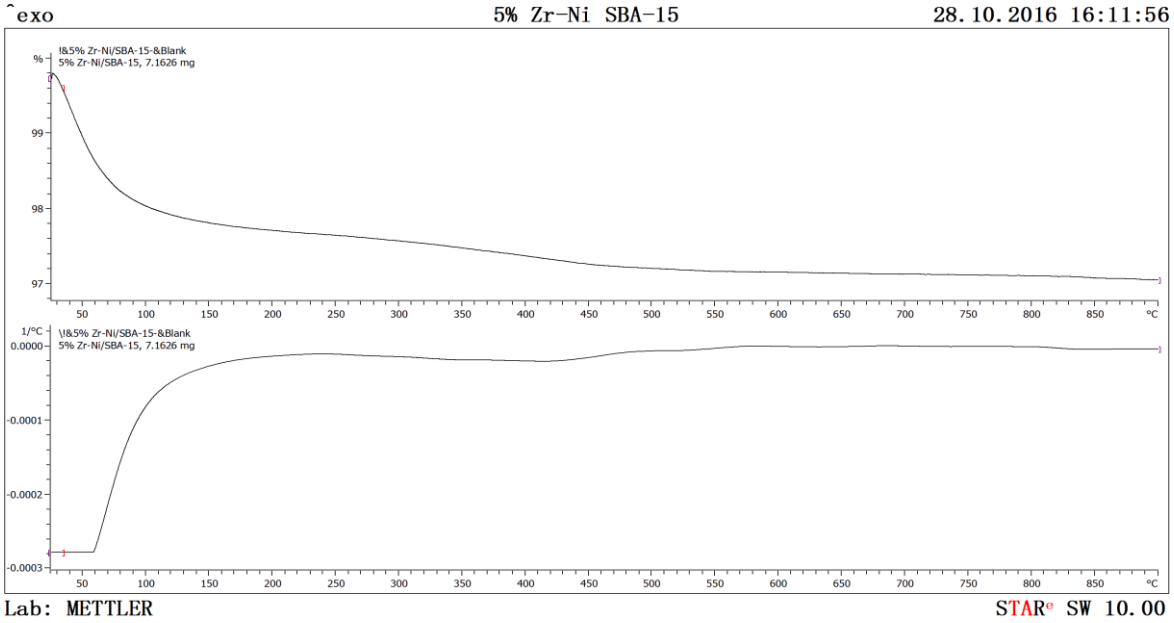

Figure 4.3 (c) shows thermogram profile for 5wt% Zr-promoted Ni/SBA-15 catalyst

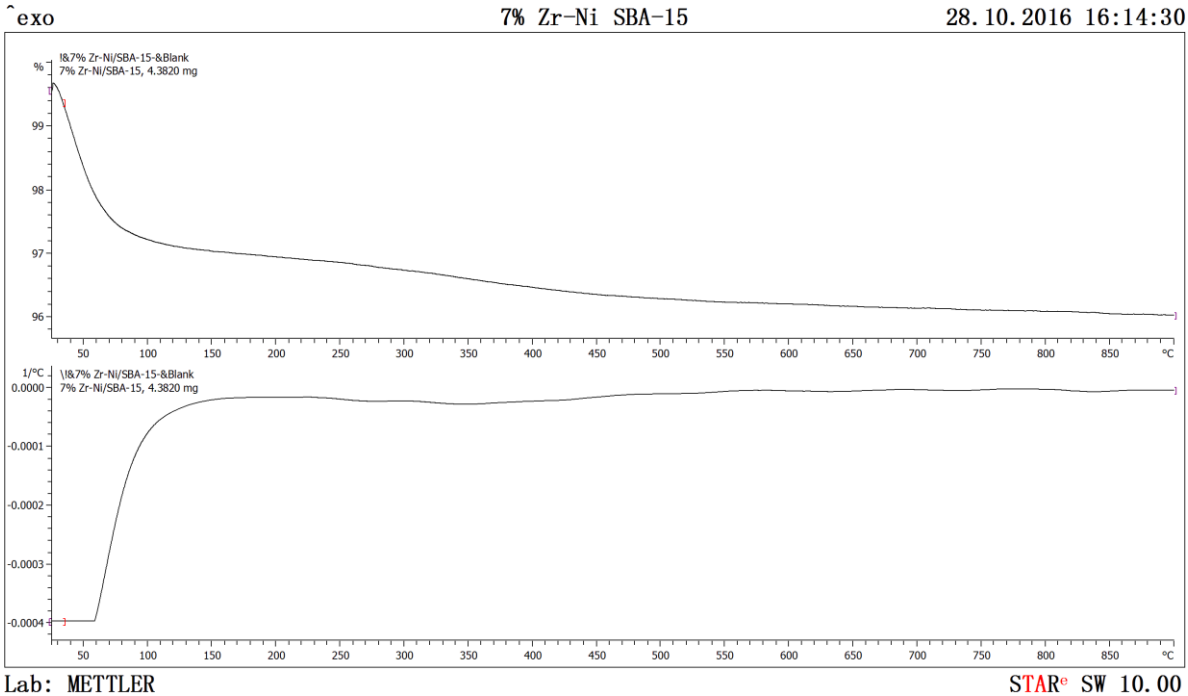

Figure 4.3 (d) shows thermogram profile for 7wt% Zr-promoted Ni/SBA-15 catalyst

Figure 4.4 shows the comparison summary graph of weight loss profile for the tested samples that occurred when the catalyst was heated up. The analysed data of all the samples of catalyst, shows almost the similar results since there is no relatively large difference in the composition. The results showed a two-weight-changing stages before a plateau was reached. The first weight change occurred from 40^{o}C to 160^{o}C which

indicated loss of surface moisture at around 40ºC and loss of inherent moisture at around 120ºC. The second weight change occurred from 250ºC to 480ºC which indicated metal nitrate decomposition *(Siew et al., 2014).* Therefore, it is determined that the first weight change stage was due to water elimination and the second weight change stage was representing the decomposition of Nickel nitrate into its oxide. The graph of weight loss profile in Figure 4.3 align with explanation which can be widely accepted.

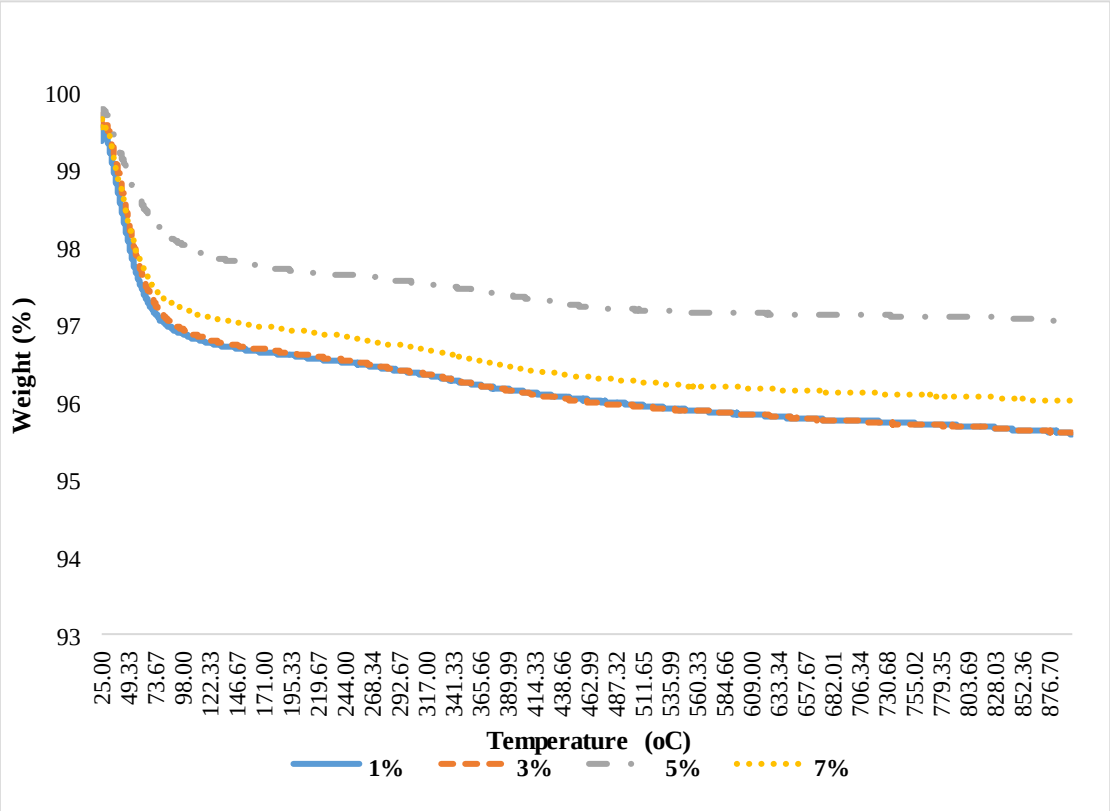

Figure 4.4 shows the comparison summary graph of weight loss profile for the tested samples

Moreover, Figure 4.5 which depicts the rate of change in weight over temperature of the researched catalysts. This graph clearly indicates the profile of weight loss at specified temperature. The weight loss profile for all the four samples reinforces the justifications done based on the thermogram. The profile for water elimination (40ºC to 160ºC) are however more obvious where surface moisture and inherent moisture losses are clearly depicted compared to the thermogram. The maximum peak (250ºC to 480ºC) represents the decomposition of Nickel Nitrate into its oxide.

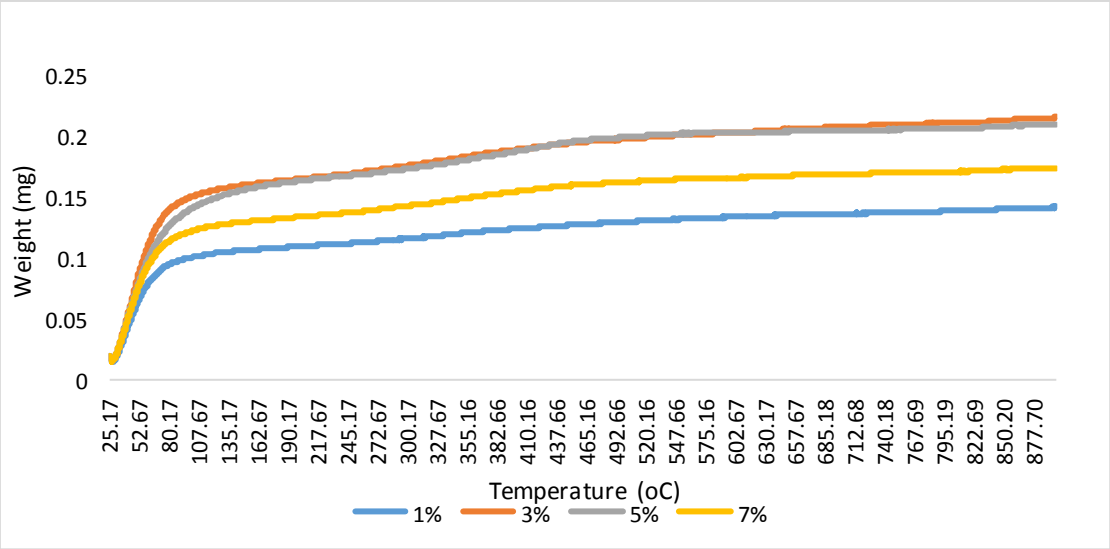

Figure 4.5 shows the rate of change in weight of samples over temperature.

4.1.4 Fourier Transform Infrared Spectroscopy (FTIR) Analysis

FTIR spectroscopy is used to identify organic, polymeric, and in some cases, inorganic materials on the Zr-promoted Ni/SBA-15 catalyst. Table 4.3 shows the functional group of chemical substances and its specific wavenumber *(Li et al.,2008).*

Table 4.3: Functional group according to wavenumber *(Li et al., 2008)*

Wavenumber (cm^{-1})	Functional Group
1030 – 1155	C-O
1550 - 1650	NH_2
600 - 400	Aromatic ring
2500 – 3500	O-H
2880 – 2500	C- H
3300 - 3500	N-H

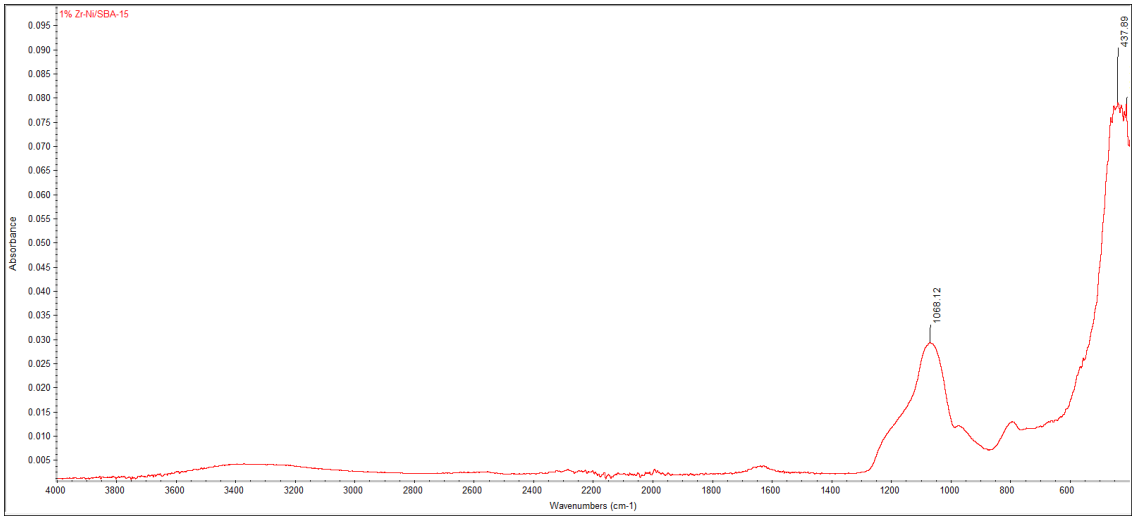

Figure 4.6 (a) shows FTIR spectrum for 1wt% Zirconium promoted Ni/SBA-15 catalyst sample

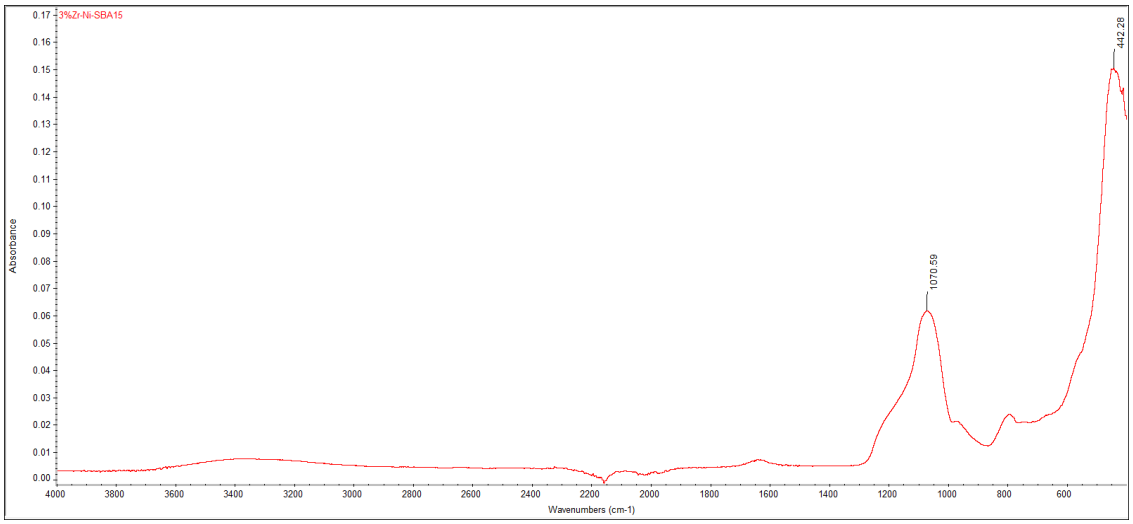

Figure 4.6 (b) shows FTIR spectrum for 3wt% Zirconium promoted Ni/SBA-15 catalyst sample

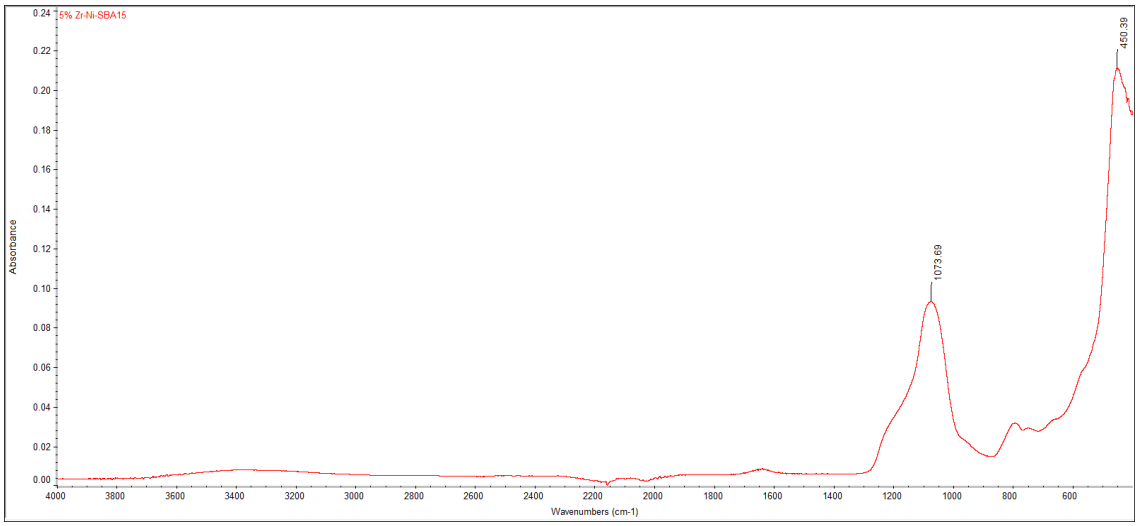

Figure 4.6 (c) shows FTIR spectrum for 5wt% Zirconium promoted Ni/SBA-15 catalyst sample

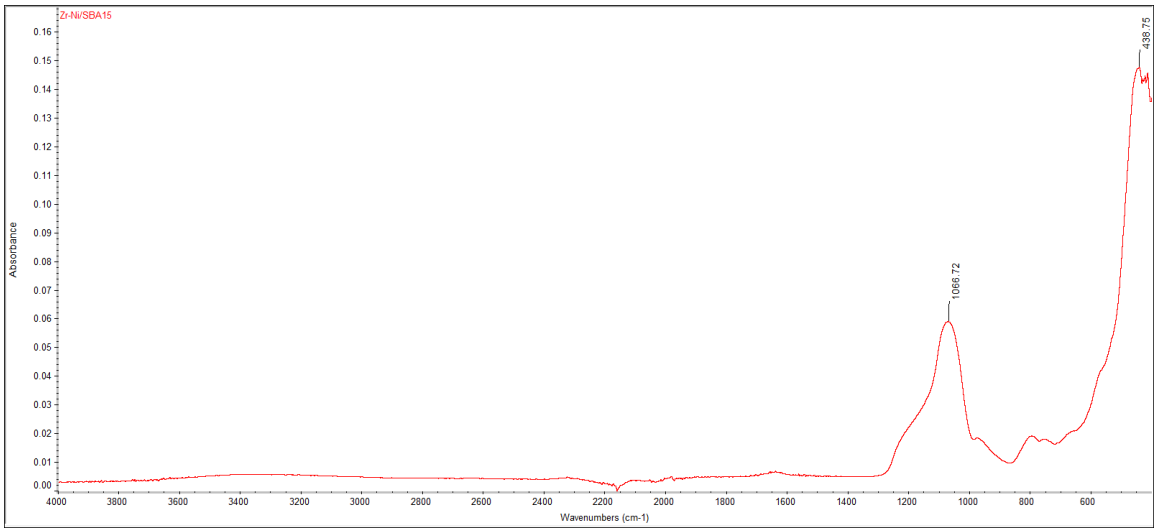

Figure 4.6 (d) shows FTIR spectrum for 7wt% Zirconium promoted Ni/SBA-15 catalyst sample

Figure 4.6 (a), (b), (c) and (d) shows FTIR spectrum for 1wt%, 3wt%, 5wt% and 7wt% of Zirconium promoted Ni/SBA-15 catalyst sample respectively. The FTIR spectroscopy analysis of the synthesized Zr-promoted Ni/SBA-15 samples has proved that in all samples the observed bands of absorption characterize the creation of Si-O-Si, Si-O-C, C-O-C and Si-C bonds. Different types of bonds, and thus different functional groups, absorb infrared of different wavelengths. Although the analysis is performed in absorbance, it can be radiation converted to transmittance, since they are simply the inversions of each other. The analytical spectrum is then compared in a reference library program with cataloged spectra to identify components or to find a “best match” for unknown material using the cataloged spectra for known materials The band around 1050 cm^{-1} to 1080 cm^{-1} could be due to the antisymmetrical stretching vibration of Si-O-Si, overlapped with Si-O-C, C-O-C and Si-C bond vibration. The Si-O-Si bond shows the polymerization of Silicate is achieved throughout the catalyst preparation. The band indicates SBA-15 support structure is present due to the vibration of Si-O-Si bond. On the other hand, the peaks around 430 cm^{-1} to 450 cm^{-1} could be assigned to associate Si-O-Si bond bending vibrations. The wavenumber increase with an increase of the Zirconium content in Zr-Ni/SBA-15. In general, the shift of this absorption band toward the higher wavenumber is considered an indication of metal incorporating into the framework of silica tetrahedral. Therefore, it indicates that the Zr may be partly incorporated into the framework of SBA-15. The explanation can be considered for all

the catalyst sample since the peaks of spectrum is the almost the same as shown in the Figure 4.7.

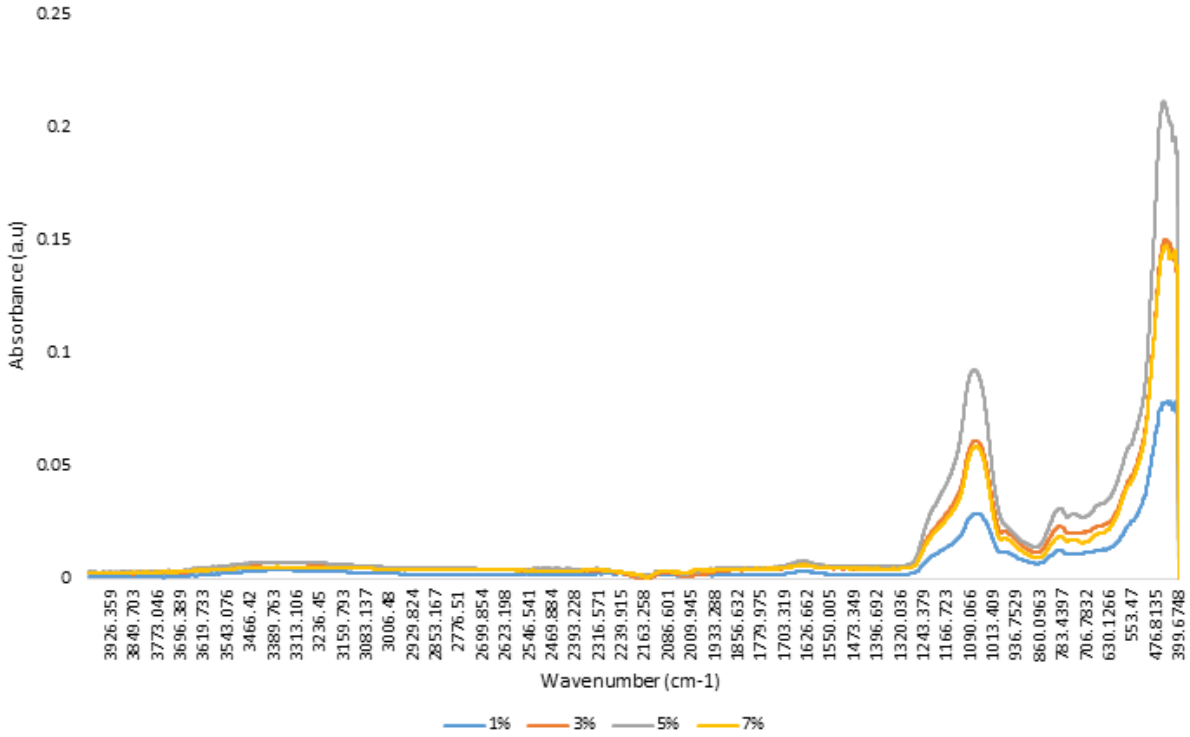

Figure 4.7 shows the comparison of FTIR spectrum for the catalyst sample

4.2 Catalytic Reaction Studies

The production of syngas from CO_2 reforming of methane has been reported by numerous researchers. CO_2 reforming of methane has been researched (Chin J Catal, 2006) by using Ni/SBA-15 as catalyst. The implementation of Zirconium series promoters on Ni/SBA-15 catalyst to generate synthesis gas discussed in this research paper. The catalytic performance of catalyst with different Zirconium loadings was evaluated in terms of gaseous product conversion and formation.

$$X_{CH4} = (F_{CH4,\,in} - F_{CH4,\,out}) / F_{CH4,\,in}$$

$$X_{CO2} = (F_{CO2,\,in} - F_{CO2,\,out}) / F_{CO2,\,in}$$

$$S_{H2} = F_{H2,\,out} / 2(F_{CH4,\,in} - F_{CH4,\,out})$$

$$S_{CO} = F_{CO,\,out} / ((F_{CH4,\,in} - F_{CH4,\,out}) + (F_{CO2,\,in} - F_{CO2,\,out}))$$

Where X is the conversion, S is the selectivity, and F is the gas flow rate ($F_i = F_{total} \cdot C_i$, where C_i is the molar fraction of the gas).

The summary of reaction data calculated using the formulas above shown in Table 4.3. Based on the Table 4.4 it was determined that the conversions of methane and carbon dioxide decrease dramatically as the percentage of Zirconium loading increases. Hence, formations of gaseous products decrease with an increase in promoter loadings. Due to inconsistency in results, a linear curve could not be obtained. Nevertheless, it is found that the highest average conversion of methane and carbon dioxide occurred at 1023K with 90.91% and 90.46% respectively. Comparisons were made in terms of percentage of Zirconium loadings for yields of products formed.

Table 4.4 Summary of reaction data of CO_2 reforming of methane for catalyst samples

Weight Percentage of Zr	CH4 Conversion (%)	CO2 Conversion (%)	H_2 Selectivity (%)	CO Selectivity (%)	H2 Yield (%)	CO Yield (%)	H_2/CO Ratio
1%	90.91	90.46	72.4164	27.5836	51.75	19.71	2.63
3%	45.0257	49.72869	45.43	54.57	13.90	13.53	0.9451
5%	30.39	32.77	44.61	55.39	11.39	14.15	0.8054
7%	30.69	37.42	38.15	61.85	8.28	12.99	0.6449

4.2.1 Effect of Zirconium Loading

The effect of percentage of Zr in the catalyst was observed in Figure 5 where the average conversion CO_2 and CH_4 was found to decrease from 1wt% of Zr to 7wt% of Zr at normalized reaction temperature of 800^oC. For the catalyst sample with 1wt% of Zr the conversion were considerably higher at 90.91% and 90.46% for CH_4 and CO_2 respectively. The sample with 3wt% shows the conversion of both reactant species reduced into half where the conversion were 45.0257% and 49.72869% for CH_4 and CO_2 respectively as an effect of increase in Zirconium content. For the catalyst sample with 5wt% and 7wt%, the conversion were almost the same below 40% for both reactant species.

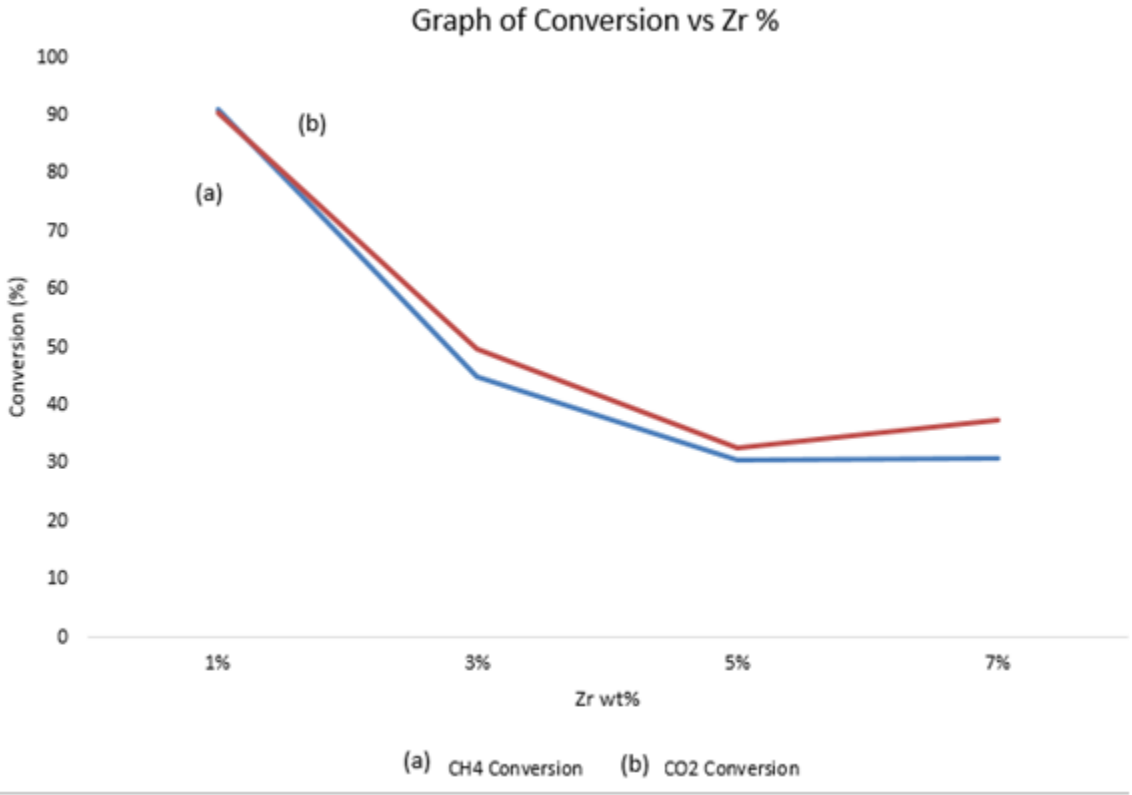

Figure 4.8 shows the conversion of CO_2 and CH_4 for different weight percentage of Zirconium promoted Ni/SBA-15 catalyst samples

The effect of percentage of Zr in the catalyst was studied in term of yield of gaseous product. In Figure 4.9, the yield profile of H_2 and CO were observed. The yield of desired product decreases as the percentage of Zr increases. At 1wt% of Zr the yield of H_2 was 51.75%, at highest value. It reduces significantly as the higher percentage of Zr in catalyst used.

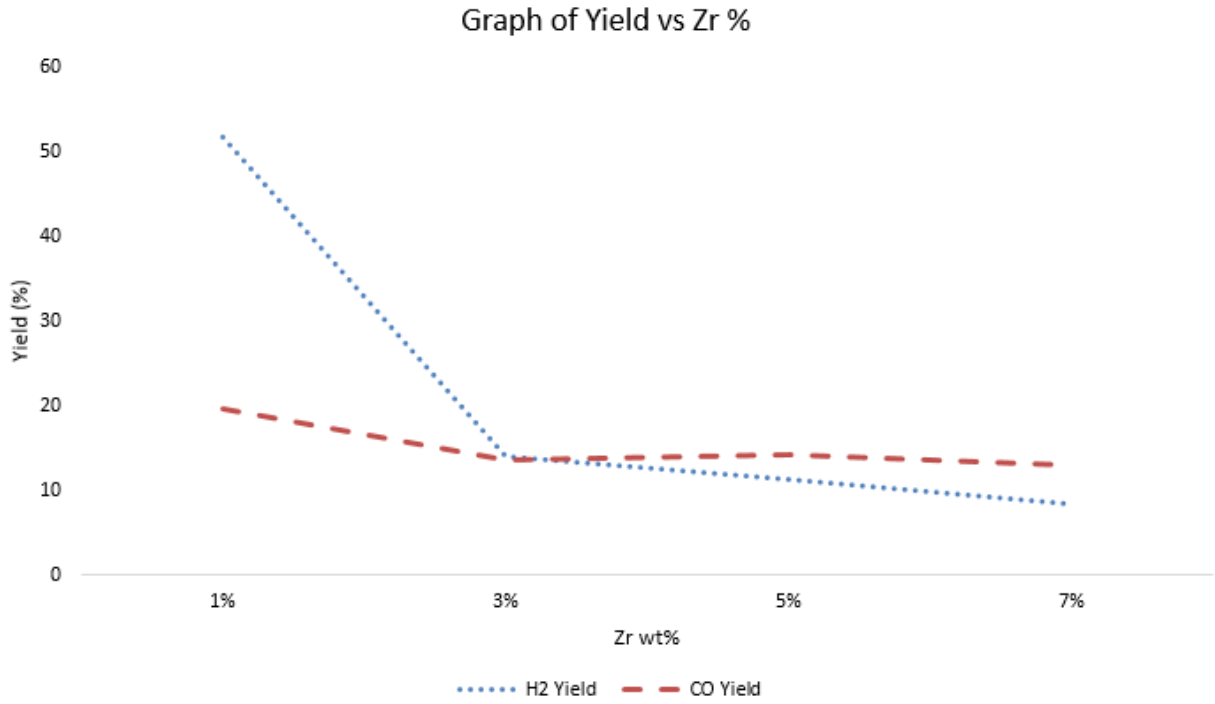

Figure 4.9 Yield profile of H_2 and CO for different weight percentage of Zirconium promoted Ni/SBA-15 catalyst samples

The Zr species enhanced the dispersion of the Ni species on the Zr-Ni/SBA-15 catalyst's surface. The introduction of promoter Zr changed the nature of the active center, promoting the formation of active center for the target reaction. Zr promoted catalyst facilitated the activation of C–H bond in CH_4. Besides, different relative proportions of carbonates were formed from CO_2 which effected the activation of CO_2 (Yao, Lu, et al, 2016). This indicates Zr-Ni/SBA-15 catalyst facilitated the activation of CO_2. Moreover, the introduction of Zr promoter led to the quicker formation and decomposition of intermediate formats *(Yao, Lu, et al, 2016).* In this study, 1wt% Zr-

promoted Ni/SBA-15 catalyst showed a higher catalytic activity for the CO_2 reforming of methane reaction than that of the non-promoted Ni/SBA-15 catalyst at normal reaction temperature.

Table 4.5 shows the comparison table of current research with previous study.

Catalyst (Process)	Conversion of CH_4 (%)	Conversion of CO_2 (%)	Researchers
12.5wt% Ni/SBA-15	89	88	Chin J Catal, 2006
1wt% Zr -12.5wt% Ni/SBA-15	90.91	90.46	Current Study

According to the table 4.5, addition of 1wt% of Zirconium promoter in the slightly increased the catalytic activity of the catalyst. While, the catalyst samples with 3wt%, 5wt% and 7wt% Zirconium promoter shows lower catalytic performance. This may due to the presence of Zirconium particles in the SBA-15. In these catalyst samples, more Zirconium species embedded into the SBA-15 mesoporous structure instead of Nickel. This might prevent more Nickel species not well dispersed and to be confined to the pores of SBA-15. This causes the sintering effect to the Nickel species at high reaction temperature of 800^{o}C. Consequently, the active site of Nickel particles aggregated during the reaction and catalyst sintering occurred which may be one cause of the catalyst deactivation *(Yao, Lu, et al. 2016).* As a result, the catalytic performance of catalyst sample with 3wt%, 5wt% and 7wt% Zirconium promoter drops dramatically. For the catalyst sample with 1wt% of promoter, Zirconium is well dispersed and promote the Nickel species to be confined to the pores of SBA-15. Thus, the Nickel species not undergone sintering as it is well embedded to SBA-15 which can withstand higher temperature *(Yao, Lu, et al, 2016).*

CHAPTER 5

CONCLUSION AND RECOMMENDATIONS

Chapter Overview

This chapter provides the overall conclusions to the current research based on significant results obtained from catalyst physicochemical studies and reaction studies of Zirconium promoted Ni/SBA-15 catalyst with different promoter loadings (1wt%, 3wt%, 5wt% and 7wt%) in CO_2 reforming of methane reaction. Besides that, recommendations for future research were also included.

5.1 Conclusion

The highly stable Zr-promoted Ni/SBA-15 catalysts with different weight percentage of Zirconium (1wt%, 3wt%, 5wt% and 7wt%) prepared by sol-gel method for CO_2 reforming of methane at 800^oC reaction temperature. 1wt% Zr-promoted Ni/SBA-15 indicates the higher catalytic performance compared to other catalyst with conversion of 90.91% and 90.46% for methane and CO_2 respectively. At high reaction temperature, SBA-15 showed good stability and limited the sintering of the Ni components. Therefore, SBA-15 is significant for the preparation of high dispersion supported catalysts and the catalytic conversion of the low-carbon alkenes. . Catalyst sample with 1wt% promoter of Zirconium is well dispersed and promote the Nickel species to be confined to the pores of SBA-15. Thus, the Nickel species not undergone sintering as it is well embedded to SBA-15 which can withstand higher temperature. In future the research can be proceeded with varying the reaction temperature and partial pressure to identify the optimum catalytic activity of the catalyst.

5.2 Recommendations

Based on the findings from this research, some suggestions are proposed in order to explore and strengthen the prospects of CO2 reforming of methane. The suggestions are as follows;

1. In the current study it is found that 1wt% of Zr-promoted Ni/SBA-15 performs with considerably high catalytic activity compared to catalyst with 3wt%, 5wt% and 7wt% of Zr-promoted Ni/SBA-15. It is suggested that further research be done to determine a more appropriate promoter weight percentage to be used to obtain the best yields *(Siew et al., 2014).* The promoter percentage can be varied from 1wt% to 3wt% in order to determine the best composition of promoter.
2. CO_2 reforming of methane has high prospects for the generation of H_2 rich syngas. The high reaction temperature is considered as the one of the significant drawback. The CO_2 reforming of methane reaction should be conducted at various temperature and partial pressure to investigate the catalytic activity of catalyst.
3. It is suggested that different types of promoters to be researched for this process as well such as other group metals such as Cerium which is considered in plenty of researches which exhibits similar characteristic as Zirconium.

REFERENCES

[1] Tang, S., Ji, L., Lin, J., Zeng, H. C., Tan, K. L., & Li, K. (2000). CO_2 reforming of methane to synthesis gas over sol–gel-made Ni/Al_2O_3 catalysts from organometallic precursors. Journal of Catalysis, 194(2), 424-430.

[2] Yao, L., Shi, J., Xu, H., Shen, W., & Hu, C. (2016). Low-temperature CO_2 reforming of methane on Zr-promoted Ni/SiO_2 catalyst. Fuel Processing Technology, 144, 1-7.

[3] Albarazi, A., Beaunier, P., & Da Costa, P. (2013). Hydrogen and syngas production by methane dry reforming on SBA-15 supported nickel catalysts: on the effect of promotion by $Ce_{0.75}Zr_{0.25}O_2$ mixed oxide. International Journal of Hydrogen Energy, 38(1), 127-139.

[4] Albarazi, A., Gálvez, M. E., & Da Costa, P. (2015). Synthesis strategies of ceria–zirconia doped Ni/SBA-15 catalysts for methane dry reforming. Catalysis Communications, 59, 108-112.

[5] Lucrédio, A. F., Jerkiewickz, G., & Assaf, E. M. (2007). Nickel catalysts promoted with cerium and lanthanum to reduce carbon formation in partial oxidation of methane reactions. Applied Catalysis A: General, 333(1), 90-95.

[6] Littlewood, P., Xie, X., Bernicke, M., Thomas, A., & Schomäcker, R. (2015). $Ni_{0.05}Mn_{0.95}O$ catalysts for the dry reforming of methane. Catalysis Today, 242, 111-118.

[7] Li, B., & Zhang, S. (2013). Methane reforming with CO_2 using nickel catalysts supported on yttria-doped SBA-15 mesoporous materials via sol–gel process. International Journal of Hydrogen Energy, 38(33), 14250-14260.

[8] Wang, N., Yu, X., Shen, K., Chu, W., & Qian, W. (2013). Synthesis, characterization and catalytic performance of MgO-coated Ni/SBA-15 catalysts for methane dry reforming to syngas and hydrogen. International journal of hydrogen energy, 38(23), 9718-9731.

[9] Wu, H., La Parola, V., Pantaleo, G., Puleo, F., Venezia, A. M., & Liotta, L. F. (2013). Ni-based catalysts for low temperature methane steam reforming: recent results on Ni-Au and comparison with other Bi-metallic systems. Catalysts, 3(2), 563-583.

[10] Ross, J. R. H., Van Keulen, A. N. J., Hegarty, M. E. S., & Seshan, K. (1996). The catalytic conversion of natural gas to useful products. Catalysis Today, 30(1), 193-199.

[11] Wang, S., Lu, G. Q., & Millar, G. J. (1996). Carbon dioxide reforming of methane to produce synthesis gas over metal-supported catalysts: state of the art. Energy & Fuels, 10(4), 896-904.

[12] BP Statistical Review of
World Energy 2015
bp.com/statisticalreview

[13] Nakamura, J., Aikawa, K., Sato, K., & Uchijima, T. (1994). Role of support in reforming of CH_4 with CO_2 over Rh catalysts. Catalysis letters, 25(3-4), 265-270.

[14] Kumar, P., Sun, Y., & Idem, R. O. (2007). Nickel-based ceria, zirconia, and ceria–zirconia catalytic systems for low-temperature carbon dioxide reforming of methane. Energy & Fuels, 21(6), 3113-3123.

[15] Li, Y., Feng, Z., Lian, Y., Sun, K., Zhang, L., Jia, G., ... & Li, C. (2005). Direct synthesis of highly ordered Fe-SBA-15 mesoporous materials under weak acidic conditions. Microporous and Mesoporous Materials, 84(1), 41-49.

[16] Ravaghi-Ardebilia, Z., Manentia, F., Pirolab, C., Soaresc, F., Corbettaa, M., Pieruccia, S., & Ranzia, E. (2014). Influence of the Effective Parameters on H_2: CO Ratio of Syngas at Low-Temperature Gasification. CHEMICAL ENGINEERING, 37.

[17] Bentley, R. W. (2002). Global oil & gas depletion: an overview. Energy policy, 30(3), 189-205.

[18] Fidalgo, B., & Menéndez, J. A. (2013). Syngas production by CO_2 reforming of CH4 under microwave heating–Challenges and opportunities.

[19] Liu, D., Quek, X. Y., Wah, H. H. A., Zeng, G., Li, Y., & Yang, Y. (2009). Carbon dioxide reforming of methane over nickel-grafted SBA-15 and MCM-41 catalysts. Catalysis Today, 148(3), 243-250.

[20] Jacobs, G., Das, T. K., Zhang, Y., Li, J., Racoillet, G., & Davis, B. H. (2002). Fischer–Tropsch synthesis: support, loading, and promoter effects on the reducibility of cobalt catalysts. Applied Catalysis A: General, 233(1), 263-281.

[21] Armor, J. N. (1999). The multiple roles for catalysis in the production of H_2. Applied Catalysis A: General, 176(2), 159-176.

[22] Song, C. (2010). Introduction to hydrogen and syngas production and purification technologies. Hydrogen and syngas production and purification technologies, 1-12.

[23] Rostrup-Nielsen, J. R., Sehested, J., & Nørskov, J. K. (2002). Hydrogen and synthesis gas by steam-and CO_2 reforming. Advances in catalysis, 47, 65-139.

[24] Dunn, S. (2002). Hydrogen futures: toward a sustainable energy system. International journal of hydrogen energy, 27(3), 235-264.

[25] Cullity, B. D., & Stock, S. R. (2001). Elements of X-ray Diffraction (Vol. 3): Prentice hall Upper Saddle River, NJ.

[26] Lachance, G. R., & Claisse, F. (1995). Quantitative X-ray fluorescence analysis: theory and application: John Wiley & Son Ltd.

[27] Jenkins, R. (2000). X-Ray Techniques: Overview. Encyclopedia of analytical chemistry

APPENDICES

Catalyst Characterization Data

1. Fourier Transform Infrared Spectroscopy (FTIR) Analysis

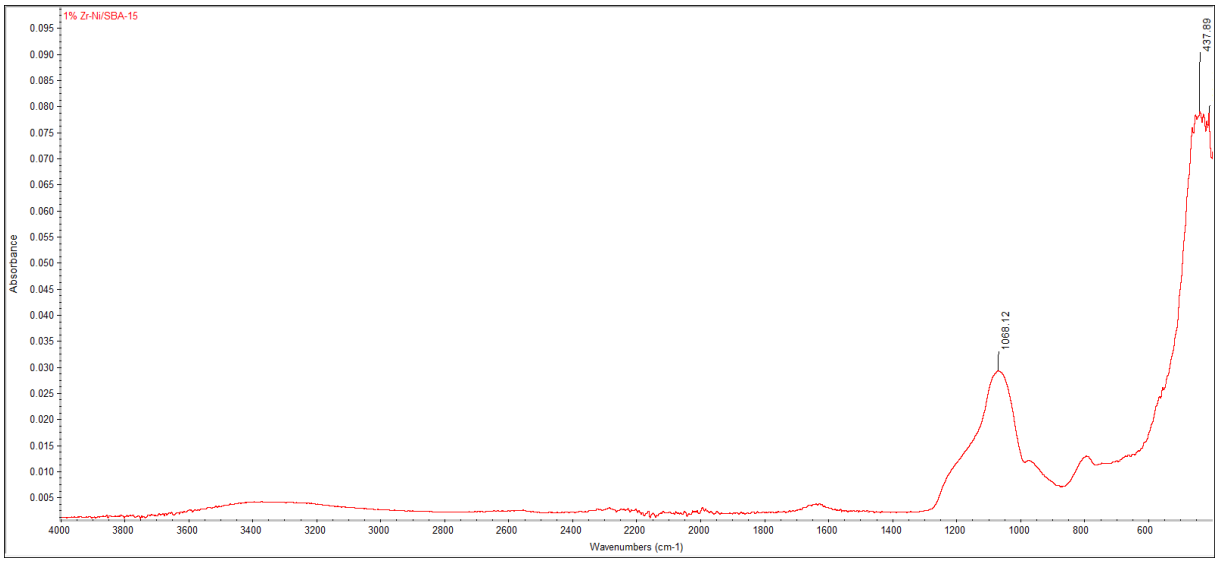

- 1wt% Zr-Ni/SBA-15

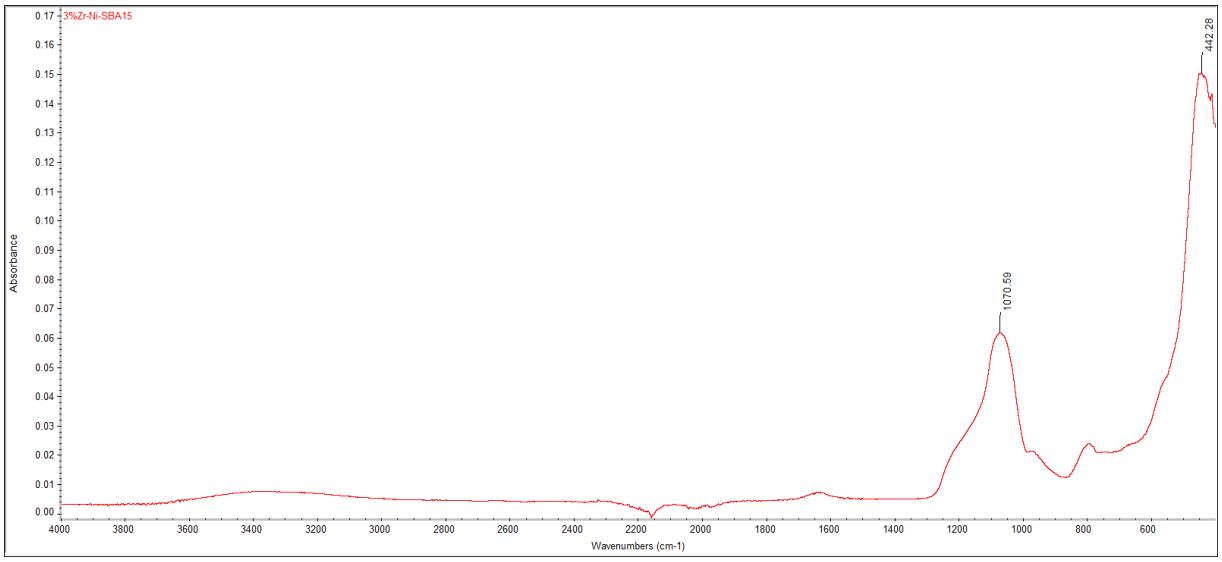

- 3wt% Zr-Ni/SBA-15

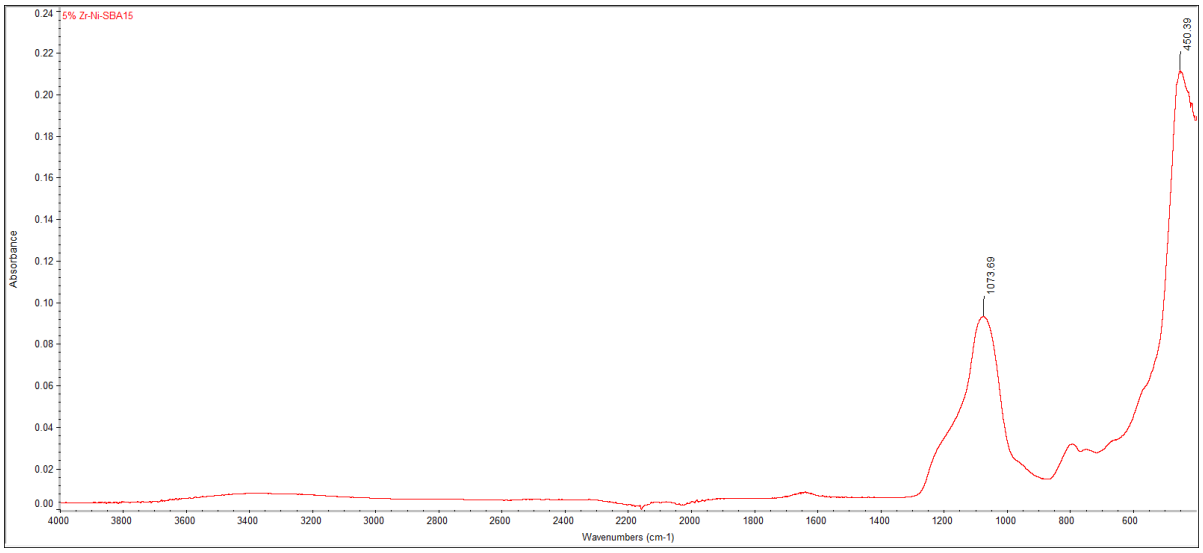

- 5wt% Zr-Ni/SBA-15

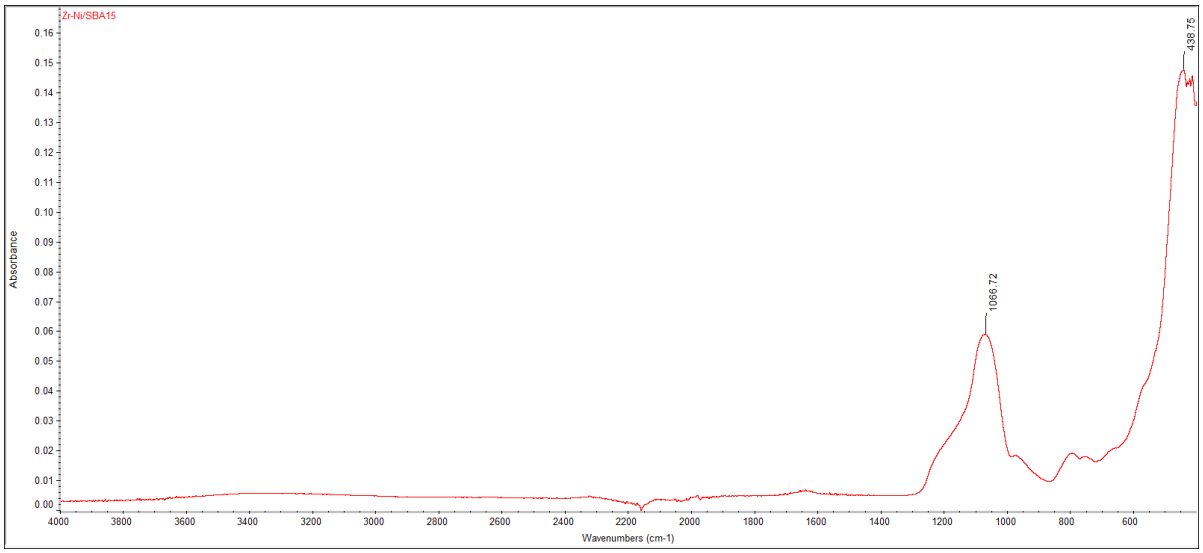

- 7wt% Zr-Ni/SBA-15

2. Brunauer-Emmett-Teller (BET) Analysis

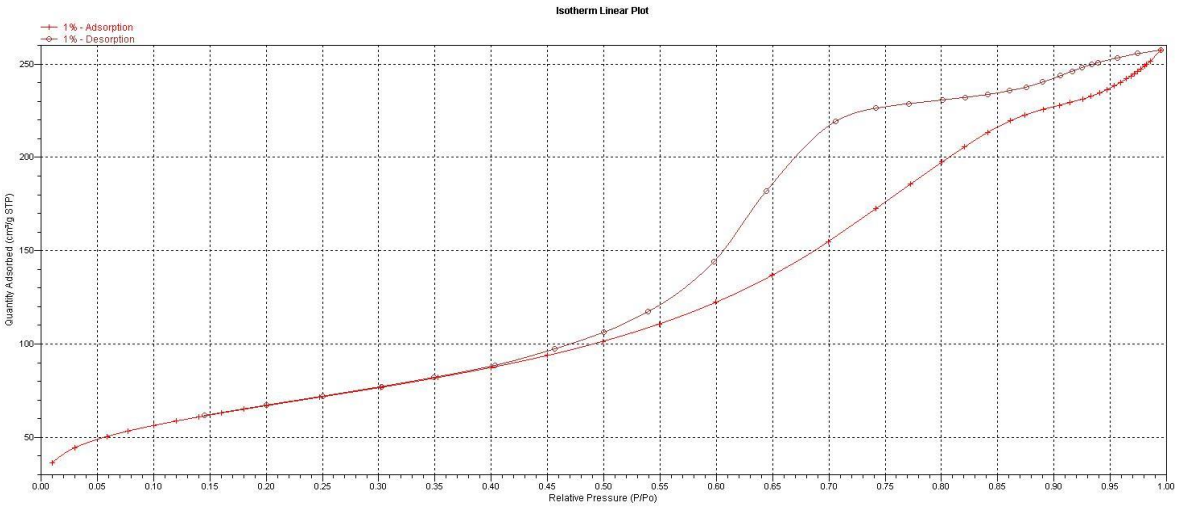

- Adsorption/desorption isotherms for 1wt% of Zr-Ni/SBA-15

Full Report Set

ASAP 2020 V3.04 H Unit 1 Serial #: 1255 Page 1

Sample: 1%

Operator: HALIM

Submitter: UMP

File: C:\2020\DATA\001-746.SMP

Started: 12/3/2016 8:25:09AM

Completed: 12/3/2016 2:41:07PM

Report Time: 12/5/2016 8:54:03AM

Sample Mass: 0.2172 g

Cold Free Space: 83.7709 cm³

Low Pressure Dose: None

Analysis Adsorptive: N2

Analysis Bath Temp.: -195.791 °C

Thermal Correction: No

Warm Free Space: 27.7172 cm³ Measured

Equilibration Interval: 5 s

Automatic Degas: Yes

Summary Report

Surface Area

Single point surface area at P/Po = 0.301716322: 233.4065 m²/g

BET Surface Area: 240.0202 m²/g

Langmuir Surface Area: 380.7260 m²/g

t-Plot Micropore Area: 5.7936 m²/g

t-Plot External Surface Area: 234.2266 m^2/g
BJH Adsorption cumulative surface area of pores between 17.000 Å and 3000.000 Å diameter: 268.521 m^2/g
BJH Desorption cumulative surface area of pores between 17.000 Å and 3000.000 Å diameter: 308.5337 m^2/g

Pore Volume

Single point adsorption total pore volume of pores less than 1376.175 Å diameter at P/Po = 0.985733818: 0.388978 cm^3/g
Single point desorption total pore volume of pores less than 770.234 Å diameter at P/Po = 0.974211070: 0.395282 cm^3/g
t-Plot micropore volume: 0.001244 cm^3/g
BJH Adsorption cumulative volume of pores between 17.000 Å and 3000.000 Å diameter: 0.411027 cm^3/g
BJH Desorption cumulative volume of pores between 17.000 Å and 3000.000 Å diameter: 0.407965 cm^3/g

Pore Size

Adsorption average pore width (4V/A by BET): 64.8243 Å
Desorption average pore width (4V/A by BET): 65.8748 Å
BJH Adsorption average pore diameter (4V/A): 61.228 Å
BJH Desorption average pore diameter (4V/A): 52.891 Å

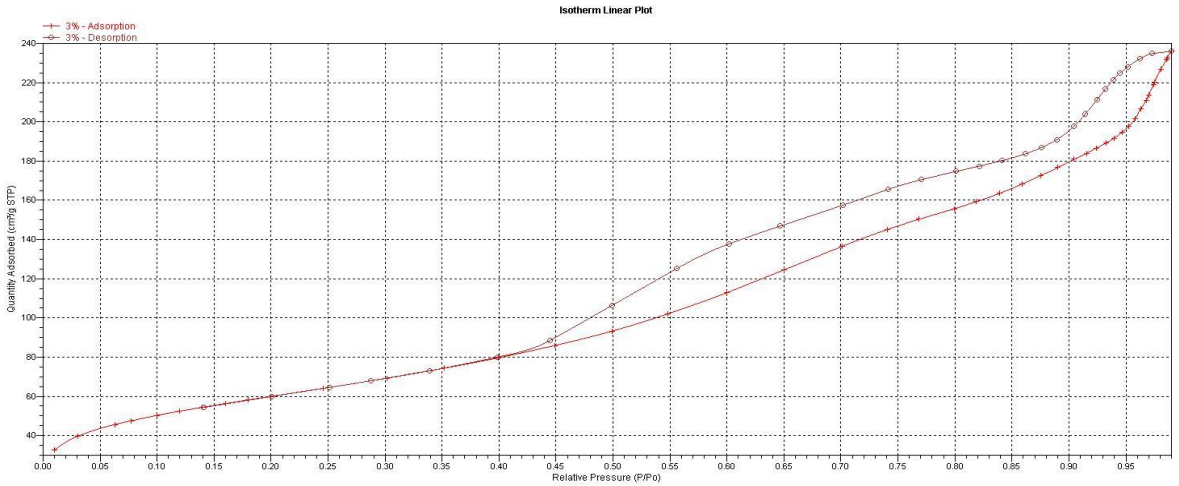

- Adsorption/desorption isotherms for 3wt% of Zr-Ni/SBA-15

Full Report Set

ASAP 2020 V3.04 H Unit 1 Serial #: 1255 Page 1

Sample: 3%

Operator: HALIM

Submitter: UMP

File: C:\2020\DATA\001-747.SMP

Started: 12/3/2016 4:48:29PM

Completed: 12/4/2016 1:29:30AM

Report Time: 12/5/2016 8:54:05AM

Sample Mass: 0.3841 g

Cold Free Space: 84.0057 cm^3

Low Pressure Dose: None

Analysis Adsorptive: N2

Analysis Bath Temp.: -195.793 °C

Thermal Correction: No

Warm Free Space: 27.7045 cm^3 Measured

Equilibration Interval: 5 s

Automatic Degas: Yes

Summary Report

Surface Area

Single point surface area at P/Po = 0.301339945: 210.6180 m^2/g

BET Surface Area: 216.8302 m^2/g

Langmuir Surface Area: 346.1452 m^2/g

t-Plot Micropore Area: 0.9261 m^2/g

t-Plot External Surface Area: 215.9041 m^2/g

BJH Adsorption cumulative surface area of pores between 17.000 Å and 3000.000 Å diameter: 242.235 m^2/g
BJH Desorption cumulative surface area of pores between 17.000 Å and 3000.000 Å diameter: 274.1664 m^2/g

Pore Volume

Single point adsorption total pore volume of pores less than 1358.632 Å diameter at P/Po = 0.985546384: 0.358385 cm^3/g
Single point desorption total pore volume of pores less than 744.721 Å diameter at P/Po = 0.973306706: 0.363167 cm^3/g
t-Plot micropore volume: -0.001522 cm^3/g
BJH Adsorption cumulative volume of pores between 17.000 Å and 3000.000 Å diameter: 0.378177 cm^3/g
BJH Desorption cumulative volume of pores between 17.000 Å and 3000.000 Å diameter: 0.375335 cm^3/g

Pore Size

Adsorption average pore width (4V/A by BET): 66.1135 Å
Desorption average pore width (4V/A by BET): 66.9956 Å
BJH Adsorption average pore diameter (4V/A): 62.448 Å
BJH Desorption average pore diameter (4V/A): 54.760 Å

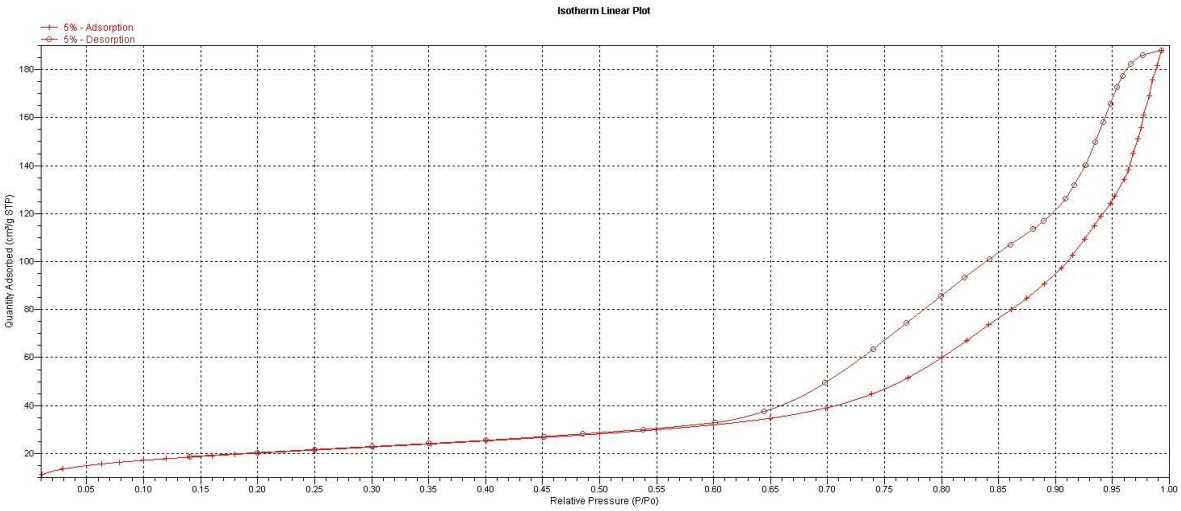

- Adsorption/desorption isotherms for 5wt% of Zr-Ni/SBA-15

Full Report Set

ASAP 2020 V3.04 H Unit 1 Serial #: 1255 Page 1

Sample: 5%

Operator: HALIM

Submitter: UMP

File: C:\2020\DATA\001-748.SMP

Started: 12/5/2016 8:19:56AM

Completed: 12/5/2016 3:34:37PM

Report Time: 12/6/2016 8:27:44AM

Sample Mass: 0.3285 g

Cold Free Space: 84.5805 cm³

Low Pressure Dose: None

Analysis Adsorptive: N2

Analysis Bath Temp.: -195.780 °C

Thermal Correction: No

Warm Free Space: 27.7073 cm³ Measured

Equilibration Interval: 5 s

Automatic Degas: Yes

Summary Report

Surface Area

Single point surface area at P/Po = 0.301510221: 69.0630 m²/g

BET Surface Area: 70.7785 m²/g

Langmuir Surface Area: 111.9386 m²/g

t-Plot Micropore Area: 4.4537 m²/g

t-Plot External Surface Area: 66.3248 m²/g

BJH Adsorption cumulative surface area of pores between 17.000 Å and 3000.000 Å diameter: 75.352 m^2/g
BJH Desorption cumulative surface area of pores between 17.000 Å and 3000.000 Å diameter: 93.7107 m^2/g

Pore Volume

Single point adsorption total pore volume of pores less than 1325.556 Å diameter at P/Po = 0.985179309: 0.271997 cm^3/g
Single point desorption total pore volume of pores less than 858.625 Å diameter at P/Po = 0.976922416: 0.287843 cm^3/g
t-Plot micropore volume: 0.002168 cm^3/g
BJH Adsorption cumulative volume of pores between 17.000 Å and 3000.000 Å diameter: 0.293035 cm^3/g
BJH Desorption cumulative volume of pores between 17.000 Å and 3000.000 Å diameter: 0.292238 cm^3/g

Pore Size

Adsorption average pore width (4V/A by BET): 153.7176 Å
Desorption average pore width (4V/A by BET): 162.6723 Å
BJH Adsorption average pore diameter (4V/A): 155.554 Å
BJH Desorption average pore diameter (4V/A): 124.741 Å

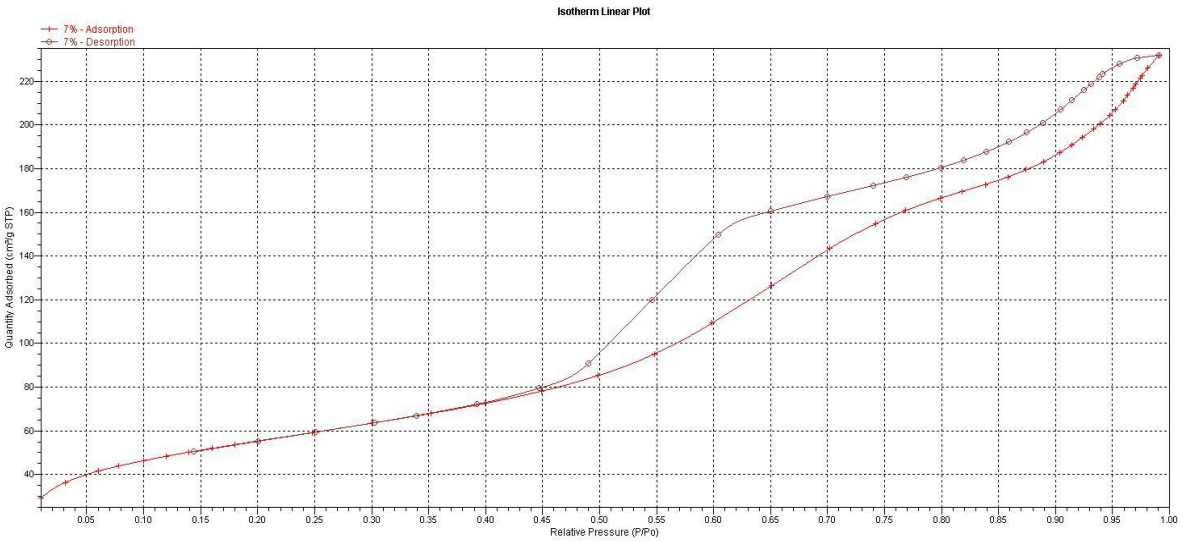

- Adsorption/desorption isotherms for 7wt% of Zr-Ni/SBA-15

Full Report Set

ASAP 2020 V3.04 H Unit 1 Serial #: 1255 Page 1

Sample: 7%

Operator: HALIM

Submitter: UMP

File: C:\2020\DATA\001-749.SMP

Started: 12/5/2016 4:06:31PM

Completed: 12/5/2016 10:17:59PM

Report Time: 12/6/2016 8:27:45AM

Sample Mass: 0.2120 g

Cold Free Space: 84.8186 cm³

Low Pressure Dose: None

Analysis Adsorptive: N2

Analysis Bath Temp.: -195.798 °C

Thermal Correction: No

Warm Free Space: 27.8067 cm³ Measured

Equilibration Interval: 5 s

Automatic Degas: Yes

Summary Report

Surface Area

Single point surface area at P/Po = 0.301180454: 193.3928 m²/g

BET Surface Area: 199.3480 m²/g

Langmuir Surface Area: 317.5708 m²/g

t-Plot Micropore Area: 0.7846 m²/g

t-Plot External Surface Area: 198.5634 m²/g

BJH Adsorption cumulative surface area of pores between 17.000 Å and 3000.000 Å diameter: 233.333 m^2/g
BJH Desorption cumulative surface area of pores between 17.000 Å and 3000.000 Å diameter: 271.0579 m^2/g

Pore Volume

Single point adsorption total pore volume of pores less than 2092.270 Å diameter at P/Po = 0.990677434: 0.358804 cm^3/g
Single point desorption total pore volume of pores less than 710.523 Å diameter at P/Po = 0.971990738: 0.356757 cm^3/g
t-Plot micropore volume: -0.001161 cm^3/g
BJH Adsorption cumulative volume of pores between 17.000 Å and 3000.000 Å diameter: 0.368307 cm^3/g
BJH Desorption cumulative volume of pores between 17.000 Å and 3000.000 Å diameter: 0.366349 cm^3/g

Pore Size

Adsorption average pore width (4V/A by BET): 71.9956 Å
Desorption average pore width (4V/A by BET): 71.5847 Å
BJH Adsorption average pore diameter (4V/A): 63.138 Å
BJH Desorption average pore diameter (4V/A): 54.062 Å

3. X-Ray Diffraction (XRD) Analysis

- **1wt% Zr-Ni/SBA-15**

Analysis date	11/5/2016 9:42:56 AM
Sample name	XRD Analysis
File name	1% Zr-Ni SBA-15.raw
Comment	UMP

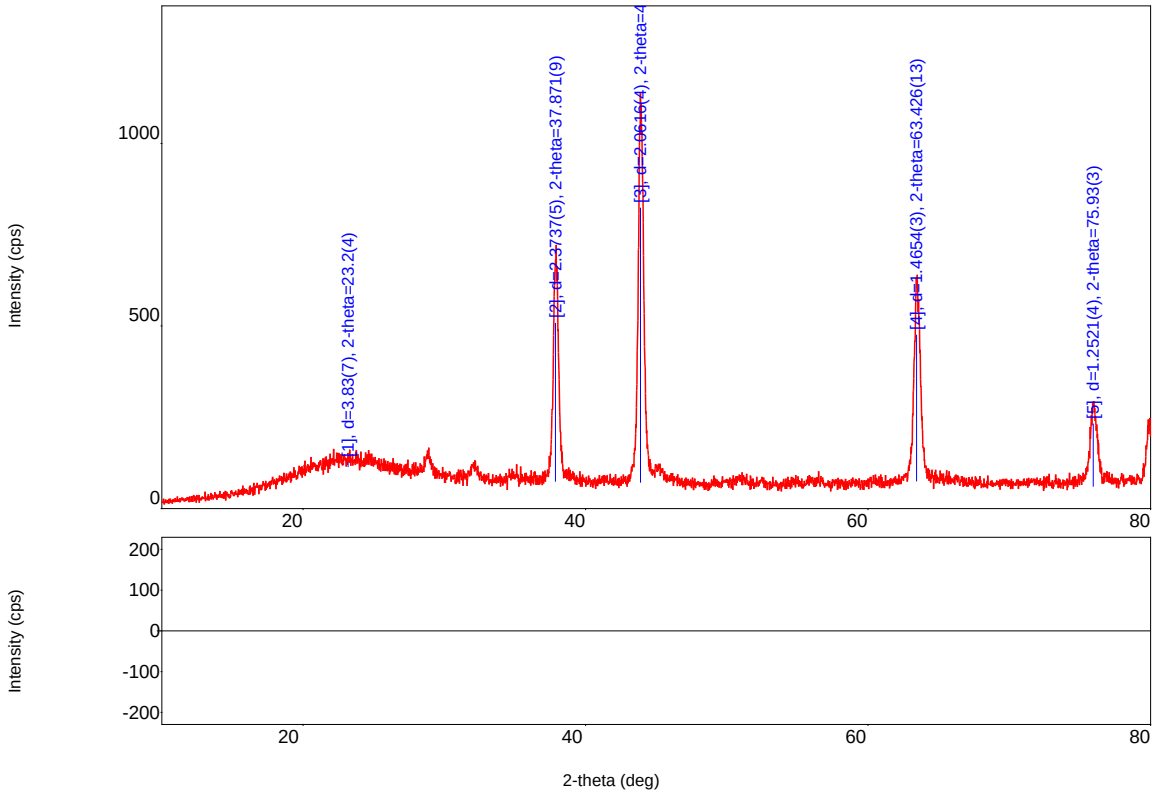

No.	2-theta(deg)	d(ang.)	Height(cps)	FWHM(deg)	Int. I(cps deg)	Size(ang.)
1	23.2(4)	3.83(7)	12(3)	5.1(4)	71(7)	16.6(13)
2	37.871(9)	2.3737(5)	433(21)	0.381(7)	203(3)	230(4)
3	43.880(8)	2.0616(4)	751(27)	0.377(6)	360(4)	237(4)
4	63.426(13)	1.4654(3)	400(20)	0.439(9)	221(3)	222(5)
5	75.93(3)	1.2521(4)	171(13)	0.46(3)	108(2)	231(13)

- **3wt% Zr-Ni/SBA-15**

Analysis date	11/5/2016 9:47:58 AM
Sample name	XRD Analysis
File name	3% Zr-Ni SBA-15.raw
Comment	UMP

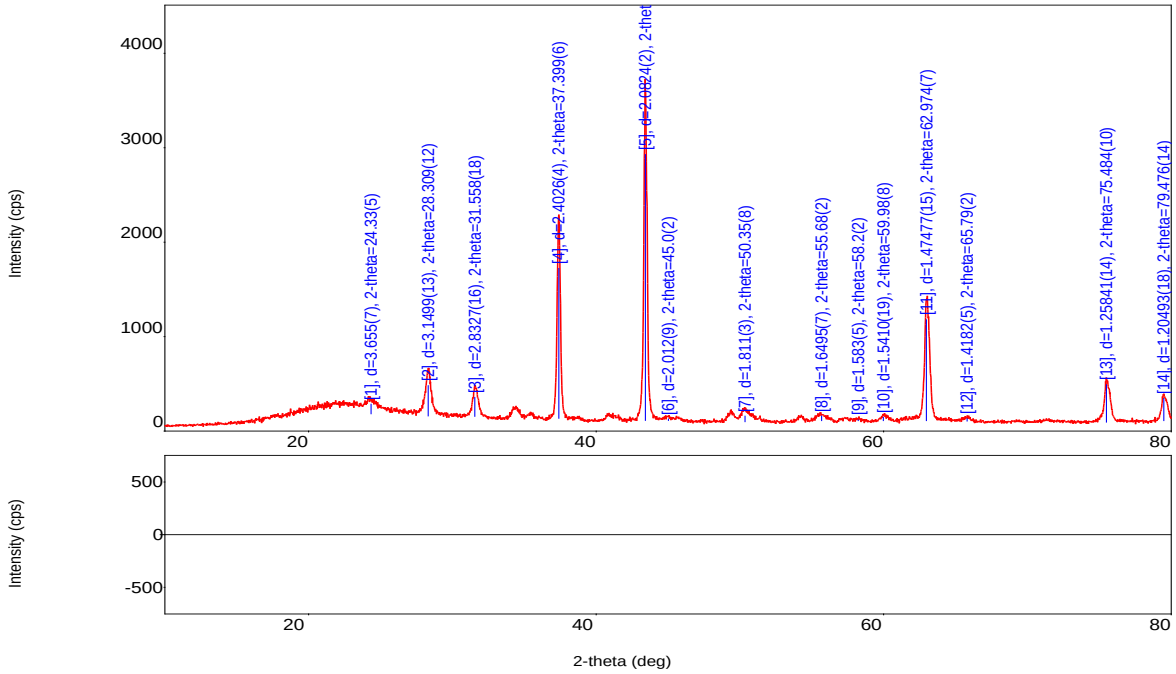

No.	2-theta(deg)	d(ang.)	Height(cps)	FWHM(deg)	Int. I(cps deg)	Size(ang.)
1	24.33(5)	3.655(7)	104(10)	2.43(11)	540(9)	34.9(15)
2	28.309(12)	3.1499(13)	323(18)	0.415(11)	186(3)	206(6)
3	31.558(18)	2.8327(16)	204(14)	0.423(15)	95(4)	204(7)
4	37.399(6)	2.4026(4)	1589(40)	0.225(4)	418(5)	389(7)
5	43.420(4)	2.0824(2)	2816(53)	0.199(4)	707(6)	449(9)
6	45.0(2)	2.012(9)	15(4)	0.85(18)	14(4)	106(23)
7	50.35(8)	1.811(3)	60(8)	1.56(7)	99(6)	59(3)
8	55.68(2)	1.6495(7)	50(7)	0.59(8)	41(3)	160(22)
9	58.2(2)	1.583(5)	10(3)	1.0(3)	13(3)	98(35)
10	59.98(8)	1.5410(19)	39(6)	0.44(6)	19(3)	215(29)
11	62.974(7)	1.47477(15)	1070(33)	0.299(6)	412(4)	326(6)
12	65.79(2)	1.4182(5)	27(5)	0.49(8)	15(2)	202(34)
13	75.484(10)	1.25841(14)	396(20)	0.300(12)	164(2)	349(14)
14	79.476(14)	1.20493(18)	236(15)	0.334(17)	93(3)	323(16)

- **5wt% Zr-Ni/SBA-15**

Analysis date	11/5/2016 9:50:02 AM
Sample name	XRD Analysis
File name	5% Zr-Ni SBA-15.raw
Comment	UMP

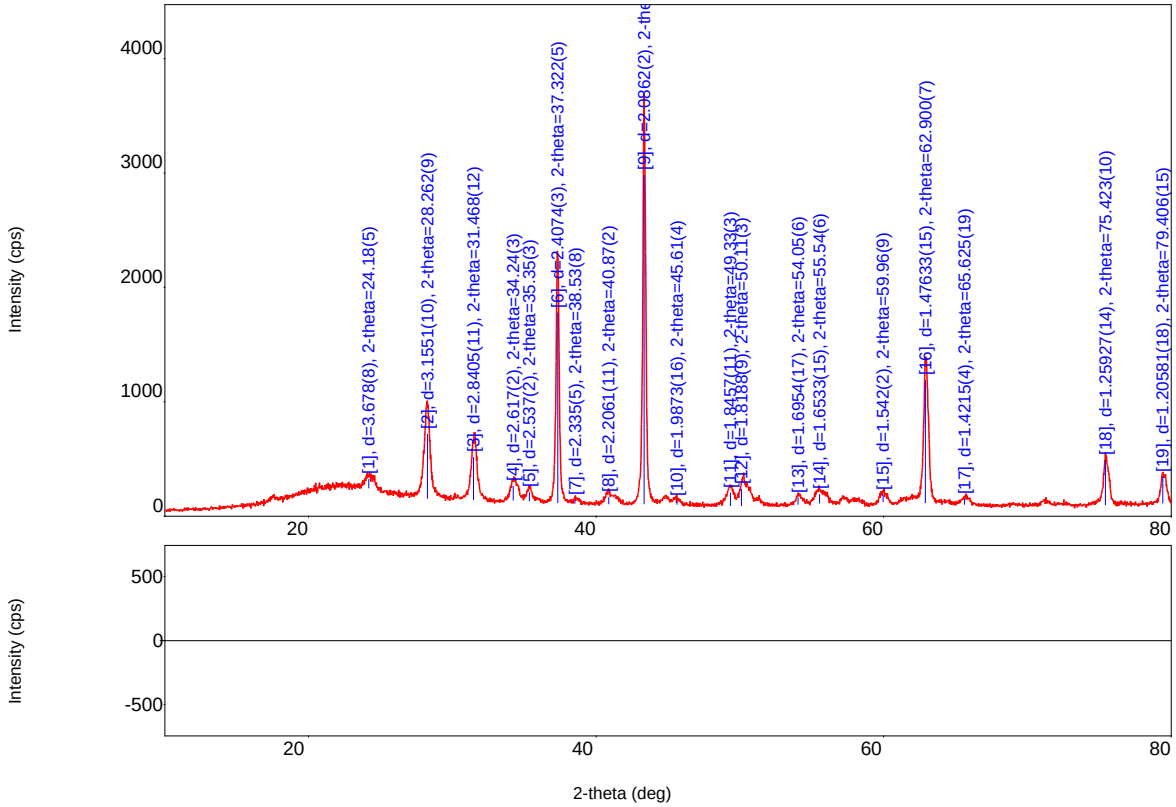

No.	2-theta(deg)	d(ang.)	Height(cps)	FWHM(deg)	Int. I(cps deg)	Size(ang.)
1	24.18(5)	3.678(8)	74(9)	0.66(5)	58(5)	128(10)
2	28.262(9)	3.1551(10)	562(24)	0.427(9)	309(4)	201(4)
3	31.468(12)	2.8405(11)	370(19)	0.433(10)	189(4)	199(5)
4	34.24(3)	2.617(2)	122(11)	0.57(3)	80(4)	152(7)
5	35.35(3)	2.537(2)	76(9)	0.36(3)	31(2)	241(23)
6	37.322(5)	2.4074(3)	1660(41)	0.202(4)	420(4)	434(9)
7	38.53(8)	2.335(5)	27(5)	0.28(6)	7.9(19)	319(70)
8	40.87(2)	2.2061(11)	56(8)	0.71(6)	43(5)	124(10)
9	43.336(4)	2.0862(2)	2870(54)	0.176(4)	651(6)	506(12)
10	45.61(4)	1.9873(16)	26(5)	1.06(13)	29(6)	85(11)
11	49.33(3)	1.8457(11)	110(11)	0.61(3)	75(3)	150(8)
12	50.11(3)	1.8188(9)	143(12)	0.85(3)	139(4)	108(3)
13	54.05(6)	1.6954(17)	56(7)	0.43(5)	26(2)	216(25)
14	55.54(6)	1.6533(15)	75(9)	0.80(5)	64(4)	118(7)
15	59.96(9)	1.542(2)	61(8)	0.39(6)	26(4)	242(40)
16	62.900(7)	1.47633(15)	1071(33)	0.270(7)	381(4)	360(9)
17	65.625(19)	1.4215(4)	42(6)	0.52(6)	25(3)	191(21)
18	75.423(10)	1.25927(14)	388(20)	0.276(13)	150(3)	381(17)
19	79.406(15)	1.20581(18)	229(15)	0.321(17)	85(3)	336(18)

- **7wt% Zr-Ni/SBA-15**

Analysis date	11/5/2016 9:51:43 AM
Sample name	XRD Analysis
File name	7% Zr-Ni SBA-15.raw
Comment	UMP

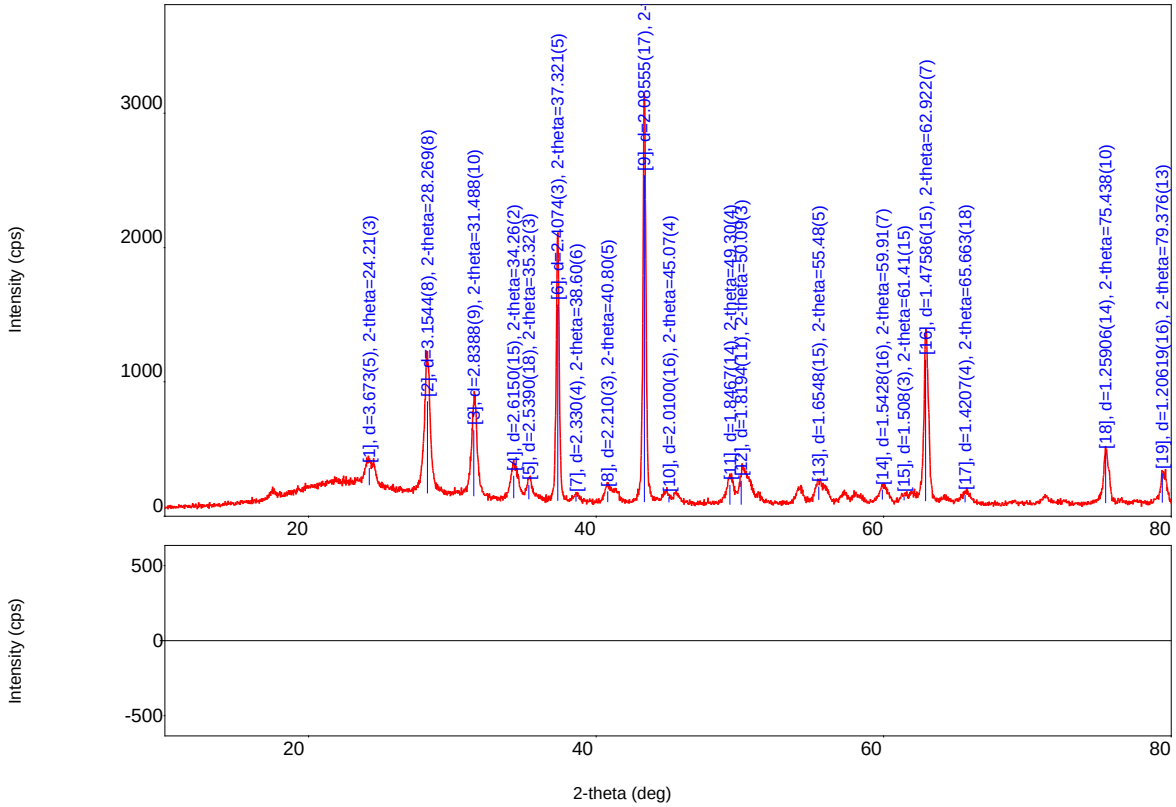

No.	2-theta(deg)	d(ang.)	Height(cps)	FWHM(deg)	Int. I(cps deg)	Size(ang.)
1	24.21(3)	3.673(5)	123(11)	0.73(3)	107(4)	117(5)
2	28.269(8)	3.1544(8)	679(26)	0.432(7)	367(4)	198(3)
3	31.488(10)	2.8388(9)	487(22)	0.417(8)	244(4)	207(4)
4	34.26(2)	2.6150(15)	163(13)	0.581(19)	107(4)	149(5)
5	35.32(3)	2.5390(18)	101(10)	0.40(3)	45(2)	219(14)
6	37.321(5)	2.4074(3)	1456(38)	0.201(4)	347(4)	435(8)
7	38.60(6)	2.330(4)	34(6)	0.33(5)	12(2)	270(40)
8	40.80(5)	2.210(3)	74(9)	0.79(4)	62(4)	112(6)
9	43.350(4)	2.08555(17)	2427(49)	0.183(3)	543(4)	489(9)
10	45.07(4)	2.0100(16)	35(6)	1.00(10)	43(3)	90(9)
11	49.30(4)	1.8467(14)	141(12)	0.55(4)	90(4)	165(11)
12	50.09(3)	1.8194(11)	172(13)	0.89(3)	171(6)	103(4)
13	55.48(5)	1.6548(15)	92(10)	0.70(6)	79(7)	134(11)
14	59.91(7)	1.5428(16)	70(8)	0.44(5)	33(4)	218(25)
15	61.41(15)	1.508(3)	21(5)	0.8(4)	20(7)	119(53)
16	62.922(7)	1.47586(15)	1047(32)	0.265(6)	340(8)	367(9)
17	65.663(18)	1.4207(4)	50(7)	0.53(5)	29(3)	187(19)
18	75.438(10)	1.25906(14)	365(19)	0.268(13)	132(3)	391(19)
19	79.376(13)	1.20619(16)	214(15)	0.283(15)	79.7(19)	381(20)